Research Square

Preprints are preliminary reports that have not undergone peer review.
They should not be considered conclusive, used to inform clinical practice,
or referenced by the media as validated information.

Fucosylation of HLA-DRB1 regulates $CD4^+$T cell-mediated anti-melanoma immunity and enhances immunotherapy efficacy

Eric Lau (Eric.Lau@moffitt.org)
H. Lee Moffitt Cancer Center & Research Institute

Daniel Lester
H. Lee Moffitt Cancer Center & Research Institute

Chase Burton
H. Lee Moffitt Cancer Center & Research Institute

Alycia Gardner
H. Lee Moffitt Cancer Center & Research Institute https://orcid.org/0000-0003-2185-5174

Patrick Innamarato
H. Lee Moffitt Cancer Center & Research Institute

Krithika Kodumudi
H. Lee Moffitt Cancer Center & Research Institute

Qian Liu
H. Lee Moffitt Cancer Center & Research Institute

Emma Adhikari
H. Lee Moffitt Cancer Center & Research Institute

Qianqian Ming
Moffitt Cancer Center

Daniel Williamson
Complex Carbohydrate Research Center, University of Georgia

Dennie Frederick
Broad Institute https://orcid.org/0000-0003-3355-5267

Tatyana Sharova
Massachusetts General Hospital

Michael White
The University of Texas MD Anderson Cancer Center https://orcid.org/0000-0001-5022-5505

Joseph Markowitz
H. Lee Moffitt Cancer Center and Research Institute

Biwei Cao
H. Lee Moffitt Cancer Center & Research Institute

Jonathan Nguyen

Department of Pathology, Moffitt Cancer Center https://orcid.org/0000-0001-6146-2047

Joseph Johnson
Moffitt Cancer Center

Matthew Beatty

Andrea Mockabee-Macias
H. Lee Moffitt Cancer Center & Research Institute

Matthew Mercurio
H. Lee Moffitt Cancer Center & Research Institute

Gregory Watson
H. Lee Moffitt Cancer Center & Research Institute

Pei-Ling Chen
H. Lee Moffitt Cancer Center & Research Institute

Susan McCarthy
H. Lee Moffitt Cancer Center & Research Institute

Carlos Moran
Moffitt Cancer Center https://orcid.org/0000-0001-8702-0554

Jane Messina
Moffitt Cancer Center

Kerry Thomas
H. Lee Moffitt Cancer Center & Research Institute

Lancia Darville
H. Lee Moffitt Cancer Center & Research Institute

Victoria Izuma
H. Lee Moffitt Cancer Center & Research Institute

John Koomen
Moffitt Cancer Center https://orcid.org/0000-0002-3818-1762

Shari Pilon-Thomas
H. Lee Moffitt Cancer Center & Research Institute

Brian Ruffell
Moffitt Cancer Center https://orcid.org/0000-0002-3846-6872

Vince Luca
Moffitt Cancer Center & Research Institute

Robert S Haltiwanger
University of Georgia https://orcid.org/0000-0001-7439-9577

Xuefeng Wang
Moffitt Cancer Center

Jennifer Wargo
MD Anderson https://orcid.org/0000-0003-3438-7576

Genevieve Boland

Massachusetts General Hospital https://orcid.org/0000-0002-7522-6173

Article

Keywords:

Posted Date: October 17th, 2022

DOI: https://doi.org/10.21203/rs.3.rs-2023267/v1

License: This work is licensed under a Creative Commons Attribution 4.0 International License.
Read Full License

Version of Record: A version of this preprint was published at Nature Cancer on January 23rd, 2023. See the published version at https://doi.org/10.1038/s43018-022-00506-7.

Abstract

Despite reports of striking outcomes, immunotherapy efficacy in melanoma is limited to subsets of patients [1, 2]. Combining immunotherapies with other modalities has yielded limited improvements but also adverse events requiring cessation of treatment [1]. In addition to ineffective patient stratification, efficacy can be impaired by paucity of tumor-infiltrating lymphocytes (TILs). Thus, effective strategies to safely increase TILs are urgently needed to improve immunotherapies [3]. Here, we report that dietary administration of the sugar L-fucose triggers $CD4^+$T cell-mediated increases in TILs, anti-tumor immunity, and enhanced immune checkpoint blockade responses. This is induced by the fucosylation and cell surface enrichment of the MHC-II protein HLA-DRB1 in melanoma. Single-cell immunofluorescent staining analysis of patient melanoma specimens demonstrates that fucosylation and fucosylated HLA-DRB1 is associated with intratumoral T cell abundance and anti-PD1 responder status. Our findings demonstrate that fucosylation is a key mediator of anti-tumor immunity, via regulation of melanoma cell surface HLA-DRB1 and induction of anti-tumor immunity, suggesting use of melanoma fucosylation as a novel strategy to stratify patients for immunotherapies. Importantly, our study suggests that L-fucose represents a powerful, non-toxic agent for safely increasing anti-tumor immunity and immunotherapy efficacy in melanoma.

Main

Immunotherapy responsiveness can be impaired by insufficient abundance and activity of tumor-infiltrating lymphocytes (TILs) [3]. Elucidating TIL biology and developing safe and effective strategies to increase TILs are crucial for improving the efficacy of immunotherapies.

Fucosylation, the conjugation of glycoproteins with the sugar L-fucose (L-fuc) at asparagine or serine/threonine residues (N- or O-linked, respectively) is mediated by 13 fucosyltransferases (FUTs) and impacts protein functions that are crucial for immune and developmental processes [4, 5]. Whereas altered fucosylation has been reported in a number of cancers, our understanding of its mechanisms and functional contributions is limited [6, 7]. We previously found that global fucosylation decreases during melanoma progression, and increased tumor fucosylation levels correlate with favorable patient survival outcomes [8]. Further, increasing melanoma fucosylation in a syngeneic mouse model reduced tumor growth and metastasis and significantly increased intratumoral immune cells (itICs). How fucosylation regulates anti-tumor immunity, however, was unknown. Here, we report for the first time that dietary L-fuc can regulate the biology and interactions between $CD4^+$T and melanoma cells, robustly inducing TILs and anti-melanoma immunity. Our findings demonstrate the ability of L-fuc to improve the efficacy of immunotherapies and identify novel fucosylation-based biomarkers that may enhance patient stratification.

Results

Increasing melanoma fucosylation impairs tumor growth and augmentsTIL abundance, particularly CD4$^+$ and CD8$^+$ T cells

We initially assessed how L-fuc-induced changes in itICs might contribute to melanoma suppression using a NRAS^{G13D}-mutant mouse melanoma (SW1) model [8, 9]. Oral L-fuc administration increased tumor fucosylation (~ 2-fold), reduced tumor growth (~ 50%), and increased total itICs (~ 10-50-fold) (including CD3$^+$ (CD4$^+$ and CD8$^+$) T, natural killer (NKs), macrophage (MΦ), dendritic (DCs), and myeloid-derived suppressor (MDSCs)-like cell subpopulations, without altering splenic lymphocyte profiles) (**Extended Data** Fig. 1a, Figs. 1a,b **and Extended Data** Fig. 1b,c, *respectively*). Of total itICs, CD4$^+$ and CD8$^+$ T cells were the most increased subpopulation (~ doubled) (Fig. 1c, d). Oral L-fuc induced similar changes in tumor fucosylation, growth, and TILs—specifically increased CD4$^+$ and CD8$^+$ T cells—in a BRAF^{V600E}-mutant mouse melanoma (SM1) model [10] (**Extended Data** Fig. 1d-j, *respectively*). In contrast, L-fuc did not reduce SW1 tumor growth in immunodeficient mice [11] (**Extended Data** Fig. 1k), confirming that the presence and activity of itICs are essential for L-fuc-triggered tumor suppression.

We confirmed an essential role for tumor-specific fucosylation by overexpressing murine fucokinase (mFuk) in SW1 melanoma cells to exclusively increase tumor fucosylation. mFuk expression alone suppressed tumor growth and increased total itICs comparably to oral L-fuc alone. Again, CD4$^+$ and CD8$^+$ T cells were the most increased itICs (**Extended Data** Fig. 1l,m **and** Fig. 1e-h). These data indicate that melanoma-specific fucosylation is an essential determinant of L-fuc-triggered itIC induction and tumor suppression, regardless of any other physiological host effects that L-fuc may elicit (e.g., microbiome or metabolic).

Correlations between tumor fucosylation and CD3$^+$T cells in humans by were assessed immunofluorescently analyzing a 42-patient melanoma microarray. Patients with higher than median tumor fucosylation levels exhibited significantly increased intratumoral CD3$^+$T cell densities (Fig. 1i), even after adjusting for potential confounding factors including age, sex, and stage (multivariable linear regression (*data not shown*)). Intriguingly, average melanoma fucosylation levels were lower in male patients (Fig. 1j) but exhibited a stronger association with intratumoral CD3$^+$T cells (Fig. 1k).

These data indicate that melanoma fucosylation significantly shapes itIC landscape, correlates with increased intratumoral CD3$^+$T cells in mice and humans, and can be boosted by oral L-fuc to increase TILs and suppress BRAF- and NRAS-mutant melanomas.

L-fucose suppresses melanomas by triggering CD4$^+$T cell-mediated increases in ITICs and altering CD4$^+$T cell biology, increasing memory CD4$^+$T subpopulations

The contribution of $CD4^+$ and $CD8^+$T cells to L-fuc-triggered tumor suppression was assessed by immunodepletion in the SW1 model. L-fucose reduced tumor growth by > 50% in control and $CD8^+$T cell-depleted mice, whereas this effect was completely abrogated by $CD4^+$T cell depletion (Fig. 1l-n; *immunodepletion confirmed by splenic profiling*, **Extended Data** Fig. 1n,o). Consistent with known roles for $CD4^+$T cells in recruiting and activating tumor suppressive TILs [12], $CD4^+$T cell-depletion also blocked L-fuc-induced increases in total itICs, including intratumoral NK, DC, and $CD8^+$T cells, observed in control mice (**Extended Data** Fig. 1p **and** Fig. 1o). Similarly, in the SM1 model, $CD4^+$ but not $CD8^+$T cell depletion abrogated L-fuc-triggered tumor suppression and increases in total itICs and itIC subpopulations (*immunodepletion confirmed by splenic profiling*, **Extended Data** Fig. 1q-w)).

Phosphoproteomic and fucosylated proteomic analyses revealed that L-fuc mechanistically regulates $CD4^+$T cell biology by significantly altering Protein Kinase A (PKA) and (to a lesser extent) actin signaling, potentially via Integrin B5, an upstream regulator of both of these pathways [13,14] that we discovered to be 1 of 5 proteins most highly bound to AAL (and likely fucosylated) in human peripheral blood monocyte (PBMC)-derived, CD3/CD28-activated $CD4^+$T cells, as well as Jurkat cells treated with L-fuc (**Extended Data** Fig. 2a-f). That integrin, PKA, and actin signaling have been reported to mediate T cell activation, motility, and immune synapse formation [15–17] suggests that L-fuc promotes T cell trafficking to the tumor, a notion confirmed using a SW1 melanoma C3H mouse model treated ± FTY720 (an inhibitor of lymph node egress [18]). Inhibition of lymph node egress completely abrogated L-fuc-triggered tumor suppression (Fig. 2a,b). Strikingly, L-fuc-triggered tumor suppression was associated with increases in intratumoral $CD4^+$T central and effector memory subpopulations that were abrogated by FTY720 (Fig. 2a,c **(**blue dashed boxes**) and Table 1**), consistent with the role that PKA plays in regulating memory phenotype in T cells [19]. Intriguingly, oral L-fuc induced significant, albeit transient, increases in intratumoral monocyte-derived DCs (moDCs) and lymph node cDC2s, which can promote memory $CD4^+$T phenotypes and crosstalk with $CD4^+$T cells to mediate tumor suppression, respectively [20–22] (Fig. 2a,c **(**orange dashed boxes**) and Table 1).** Finally, L-fuc also transiently but significantly increased cytotoxic $CD4^+$T cells at the midpoint (Day 28) of the experiment (Fig. 2d,e**).**

These data confirmed that $CD4^+$T cells play a key role in induction of TILs and suppression of melanomas by L-fuc, suggesting that L-fuc triggers key changes in $CD4^+$T signaling and biology at the tumor and lymph node levels that are important for tumor suppression. Importantly, that mFUK expression alone in melanoma cells resulted in smaller tumors with increased TILs (Figs. 1e-h) suggests that melanoma-specific fucosylated protein(s) can also promote anti-tumor immunity, although the mechanism was unclear.

Fucosylated HLA-DRB1 mediates L-fucose-triggered TIL induction, anti-melanoma immunity, and melanoma suppression

To identify melanoma proteins that contributed to fucosylation-triggered, $CD4^+$T cell-mediated melanoma suppression, we subjected fucosylated proteins from human melanoma cells to liquid chromatography mass spectrometric (LC-MS/MS) analysis followed by Ingenuity Pathway Analysis [23] (**Extended Data** Fig. 3a, *left*). These analyses identified "*Antigen presentation pathway*" as the only immune-related pathway, in which the MHC-I and MHC-II proteins HLA-A and HLA-DRB1, respectively, were identified as the only antigen presentation and plasma membrane proteins with T cell-modulating functions [24, 25] (**Extended Data** Fig. 3a, *right*). We confirmed their expression in human melanocytes and melanoma cells by immunoblot (IB) analysis (Fig. 3a). Further, lectin pulldown (LPD) using *Aleuria aurantia* (AAL) and *Ulex europaeus agglutinin* I (UEA1) lectins, which bind to common core and terminal fucosylated glycans, respectively [26–31], revealed association of both proteins with AAL (and to a lesser extent, UEA1), suggesting N'-linked core glycosylation-fucosylation (Fig. 3b). Finally, immunoprecipitation (IP) and IB analysis of V5-tagged HLA-A or HLA-DRB1 revealed direct recognition of HLA-DRB1 by AAL—indicating that a fraction of total HLA-DRB1, but not HLA-A, is directly fucosylated in melanoma (Fig. 3c).

To determine contributions of HLA-A or HLA-DRB1 to fucosylation-triggered anti-tumor immunity, we knocked down their C3H/HeN mouse orthologs H2K1 or EB1 [32], respectively, in SW1 tumors (**Extended Data** Fig. 3b) and assessed growth and TILs *in vivo*. Whereas L-fuc impaired control tumor growth, H2K1 knockdown suppressed tumor growth regardless of L-fuc (Fig. 3d,e), potentially reflecting tumor-protective, immunosuppressive roles of MHC-I proteins [33–35]. Notably, EB1 knockdown completely abolished L-fuc-triggered tumor suppression and induction of total itICs, including DCs, $CD8^+$ and $CD4^+$T cell subpopulations (Fig. 3f-h)—similar to the effects elicited by $CD4^+$T cell depletion (Fig. 1l-o).

Consistent with roles of HLA-DRB1 in $CD4^+$T cell activation [36–38], our findings demonstrate that HLA-DRB1 is expressed and fucosylated in melanoma and required for L-fuc-triggered $CD4^+$T cell-mediated TIL induction and melanoma suppression.

N48 fucosylation of HLA-DRB1 regulates its cell surface localization and is required for TIL induction, anti-melanoma immunity, and melanoma suppression

We reasoned that determining how HLA-DRB1 is regulated by fucosylation would provide important insight into its crucial role in L-fuc-triggered anti-tumor immunity. Using NetNGlyc and NetOGlyc (https://services.healthtech.dtu.dk) [39], we predicted N- and O-linked glycosylation sites at Asn48 (N48) and Thr129 (T129), respectively, which are conserved sites within constant regions of human and mouse HLA-DRB1 (Fig. 4a, *upper*) [32, 40]. Importantly, EB1 exhibits ~ 80% sequence homology of HLA-DRB1 and contains the conserved glycosylation-fucosylation site a N46 [32]. Modeling of HLA-DRB1 interactions with prominent binding partners HLA-DM or CD4/TCR suggests that fucosylation of neither site affects interaction interfaces or peptide loading/presentation (Fig. 4a, *lower*).

Nano-LC/MS/MS analysis of HLA-DRB1 immunoprecipitated from WM793 cells identified the fragment FLEYSTSECHFFNGTER as glycosylated-fucosylated at N48 with the predicted glycan HexNAc(4)Hex(3)Fuc(1) (Fig. 4b **and Extended Data** Fig. 4a). We mutated N48 or T129 to Gly or Ala, respectively, to abolish and verify fucosylation [41–44]. Unlike wild-type (WT) or the T129A "glyco-fucomutant" HLA-DRB1, the N48G glyco-fucomutant did not bind to AAL in LPD assays (Fig. 4c**)**, confirming fucosylation at N48 on an N-linked glycan.

To determine how fucosylation might regulate HLA-DRB1, we assessed its subcellular localization in WM793 cells that were pharmacologically modulated for fucosylation by treatment with 2F-peracteyl-fucose (FUTi, a fucosyltransferase inhibitor[45]) versus vehicle (dimethylsulfoxide, DMSO; control). Cells treated with FUTi exhibited dimmer, more central, endoplasmic reticulum-co-localization of HLA-DRB1 compared with vehicle-treated cells, suggesting less accumulation at the cell surface (Fig. 4d). Further, flow cytometry revealed that cell surface fucosylation and HLA-DRB1 both decreased or increased after FUTi or L-fuc treatments, respectively, whereas mRNA and protein levels remained unchanged; thus fucosylation promotes cell surface localization of HLA-DRB1 (Fig. 4e **and Extended Data** Fig. 4b). Finally, global proteomic profiling to identify interactors that might mediate fucosylation-regulated cell surface localization of HLA-DRB1 revealed that N48 glycosylation-fucosylation promotes binding to calnexin, which has been reported to mediate maturation and trafficking of MHC-II complexes to the surface [46] (**Extended Data** Fig. 5a-d).

To assess how HLA-DRB1 glycosylation-fucosylation contributes to tumor suppression and TILs, we compared control- or EB1-knocked-down SW1 tumors reconstituted with WT or glyco-fucomutant (N46G) EB1 (*confirmation of knockdown-reconstitution and fucosylation by IB and LPD, respectively in* **Extended Data** Fig. 5e). Abrogation of L-fuc-induced TIL and tumor growth suppression by EB1 knockdown was rescued by reconstitution with only WT but not glyco-fucomutant EB1, demonstrating that glycosylation-fucosylation of EB1/HLA-DRB1 is essential for L-fuc-triggered TIL induction and melanoma suppression (Fig. 4f **and Extended Data** Fig. 5f,g**)**. This is consistent with our finding that loss of glycosylation-fucosylation of HLA-DRB1/EB1 abrogates its cell surface localization and impairs its ability to induce anti-tumor immunity. Thus, despite the other fucosylated proteins identified in melanoma cells (**Extended Data** Fig. 3), these data confirm that the N48 glycosylation-fucosylation of HLA-DRB1 is a key regulator of anti-melanoma immunity and tumor suppression. Despite other potential host physiological effects of dietary L-fuc (e.g., microbiome, metabolome, etc.), these data confirm that L-fuc-induced itIC increases and melanoma suppression are critically mediated by melanoma-intrinsic expression and fucosylation of HLA-DRB1, which promotes its cell surface accumulation to trigger $CD4^+$T cell-mediated anti-tumor immune responses.

Oral L-fucose augments anti-PD1-mediated melanoma suppression

Expression of MHC-II reportedly correlates with increased anti-PD1 efficacy [47, 48]. Indeed, patients who failed anti-PD1 exhibited relative > 45% reduced cell surface MHC-II but not MHC-I (**Extended Data**

Fig. 5h). As anti-PD1 efficacy can be limited by TIL abundance [49], particularly of $CD4^+$T and memory $CD4^+$T cells [50–55], we tested if the ability to increase $CD4^+$T cell-mediated TIL induction and tumor suppression using oral L-fuc could be leveraged to augment anti-PD1 efficacy. In the SW1 model, oral L-fuc suppressed tumors as much as anti-PD1 but did not enhance efficacy of anti-PD1 (~ 50–60%; Fig. 5a (*left*)). In contrast, in the SM1 model, L-fuc was less tumor suppressive than anti-PD1 alone but rather augmented durable suppression in combination with anti-PD1 (Fig. 5a (*right*)).

To clarify how the L-fuc + anti-PD1 combination enhanced suppression, we characterized immune cell profiles in the tumors and lymph nodes of SM1 tumor-bearing mice over a timecourse of treatment with L-fuc ± anti-PD1. Administration of L-fuc (i) alone increased intratumoral $CD4^+$T central and effector memory cells, an effect that was increased when combined with anti-PD1 (Fig. 5b (blue dashed boxes)), and (ii), initially expanded intratumoral cDC2s, followed by later expansion of cDC2s and moDCs in the lymph nodes when combined with anti-PD1 (Fig. 5b (orange dashed boxes)). In addition to expanding the absolute numbers of intratumoral $CD4^+$ and $CD8^+$ T cells at endpoint (Day 63), combination L-fuc + anti-PD1 increased the relative percentage of intratumoral $CD8^+$T central memory cells (Fig. 5b (green dashed box)). Thus, L-fuc can suppress some melanomas as effectively as anti-PD1, whereas in others, it can enhance efficacy, which is associated with increased intratumoral $CD4^+$T central and effector memory subpopulations and lymph node cDC2 and moDC populations, consistent with the effects of L-fuc observed in Fig. 2.

Melanoma fucosylation and fucosylated HLA-DRB1 as potential biomarkers of anti-PD1 response

Given the potent enhancement of anti-PD1 efficacy by oral L-fuc in mice, we assessed if tumor fucosylation or total/fucosylated HLA-DRB1 might correlate at all with responsiveness to anti-PD1 in human patient biopsies, as the identification of preliminary correlations might support their subsequent development in into predictive biomarkers for anti-PD1 responsiveness. To this end, we devised a new technique: we modified conventional proximity ligation assay (PLA) [56] to facilitate immunofluorescent visualization of fucosylated HLA-DRB1 by implementing anti-HLA-DRB1 antibody together with biotinylated AAL, which has previously been successfully used to stain tissues specifically for core-fucosylated glycans [57] (Fig. 6a). This technique, lectin-mediated PLA (L-PLA), revealed cytoplasmic/membranous localization of endogenous fucosylated HLA-DRB1 in melanoma cells (Fig. 6b) that is lost upon FUTi treatment (Fig. 6c), confirming L-fuc-stimulated cell surface localization of HLA-DRB1 **(**Fig. 4d,e **and Extended Data** Fig. 4b). The cytoplasmic/"vesicular-appearing" staining is consistent with HLA-DRB1 that was fucosylated in the ER/Golgi and is en route to the surface via the secretory pathway. In applying this technique further on FFPE melanoma tissue specimens, we observed similar staining patterns for fucosylated HLA-DRB1 (Fig. 6d,e), which were completely abolished by L-fuc washing of the tissue, confirming specificity for fucosylated HLA-DRB1 (Fig. 6f).

To assess correlations of (i) tumor-specific fucosylation and total/fucosylated HLA-DRB1 of individual tumor cells, and (ii) intratumoral numbers $CD4^+$T cells with responder status to single-agent anti-PD1, we

implemented L-PLA on primary melanoma biopsies from 2 distinct responder and 2 non-responder patients followed by single-cell segmented signal quantitation (Fig. 7a,b). Tumors of responders clearly contained tumor cell populations with high levels of fucosylation and total HLA-DRB1 versus non-responders (Fig. 7b.**i,b.ii)**. Although the tumor of only 1 of 2 responders contained melanoma cells with increased levels of fucosylated HLA-DRB1 compared with the non-responders (Fig. 7b.**iii**), this trend mirrored that of intratumoral $CD4^+$T cell counts (Fig. 7b.**iv**), consistent with the role for fucosylated HLA-DRB1 in $CD4^+$T cell-mediated tumor suppression.

We assessed potential associations between tumor fucosylation, total/fucosylated HLA-DRB1, $CD4^+$T cells and responder status in expanded cohorts of anti-PD1-treated melanoma patients. Levels of tumor fucosylation and total and fucosylated HLA-DRB1 in tumor cells were generally higher in anti-PD1 responders compared with non-responders from Massachusetts General Hospital (n = 31; Fig. 7c, *upper*) and MD Anderson Cancer Center (n = 11; Fig. 7c, *lower*). Total tumor fucosylated HLA-DRB1 exhibited weak or no association with tumoral $CD4^+$T cell (Figs. 7d, upper & lower), although the association was modestly increased when restricted to $CD4^+$T cells localized at the periphery of the tumors (**Extended Data** Fig. 6a,b; absolute $CD4^+$T numbers **in Table 3**). The lack of significant correlation may be attributed to the dynamic relationship between fucosylated HLA-DRB1 and $CD4^+$T infiltration that is further weakened by suboptimal inclusion criteria/patient stratification. Comparison of these markers in 5 patient-matched pre- and post-anti-PD1 tumors revealed no significant correlation in total HLA-DRB1 levels. However, prior to treatment, tumor cell fucosylation was significantly higher in the complete responder versus partial and non-responders; this dropped to the equivalently lower levels of the other patients after treatment. With the exception of 1 non-responder, the complete responder also exhibited significantly increased fucosylated HLA-DRB1 in tumor cells prior to treatment (**Extended Data** Fig. 6c). The consistent trends in tumor fucosylation and fucosylated tumor HLA-DRB1 that observed across the 3 independent cancer center cohorts appear to support potential utility but importantly point to the need for further study in expanded patient pre-treatment biopsy cohorts that are controlled for a number of specific clinical variables, which will be discussed below.

Discussion

For the first time, we report the administration of a dietary sugar as a way to increase TILs and enhance efficacy of the immune checkpoint blockade agent anti-PD1. These studies reveal new insights into the post-translational regulation and immunological roles of melanoma cell-expressed MHC-II proteins, further highlighting their relationship with TILs [47, 48, 50–54]. Specifically, fucosylation regulates the cell surface abundance of HLA-DRB1, which triggers robust $CD4^+$T cell-mediated TIL induction and melanoma suppression. It is important to acknowledge that our reliance on AAL lectin predominantly focuses our study on α1,6-fucosylated proteins. Although this does not diminish the crucial role that α1,6-fucosylated HLA-DRB1—which was identified as fucosylated via lectin-agnostic click chemistry mass spectrometric screening—plays in L-fuc-triggered anti-tumor immune responses, it is possible that proteins with other fucosylation linkages might contribute to aspects of anti-tumor immunity. It is also

likely that the statistical strength of our analyses of tumor fucosylation with patient outcomes (Fig. 7) was limited by use of only AAL lectin, which precludes the detection of other structural forms of fucosylation. Nonetheless, the ability to leverage this mechanism using oral L-fuc may help to enhance other immunotherapeutic modalities (i.e., other checkpoint inhibitors or adoptive cell transfer therapies). Notably, as a non-toxic dietary sugar with a past safety precedent as an experimental therapy for children with Leukocyte Adhesion Deficiency II [58, 59], L-fuc appears to be a potentially safe and tolerable therapeutic agent.

The consistent trends that we observed in higher tumor fucosylation and fucosylated HLA-DRB1 across anti-PD1 responders vs. non-responders between the 3 independent cancer center cohorts support their potential utility as biomarkers of anti-PD1 responsiveness. However, further analyses in expanded patient biopsy cohorts are clearly needed. Considering the variable tumor suppressive effects of L-fuc observed in our anti-PD1 treated SM1 and SM1 mouse models, there are likely similar biological and clinical variables in patients that must be further explored and that may have precluded statistical significance in our small analyses.

In terms of biological variables, how T cell biology is regulated by fucosylation, for example, has heretofore been unclear. Reported divergent effects of fucosylation on T cell activation vs. exhaustion (i.e., via regulation of Programmed Death Ligand 1 (PD-L1) expression) point to FUT-specific expression and roles that remain to be elucidated [60–62]. L-fucose does not alter cell surface levels of PD-L1 in human or mouse melanoma cells (**Extended Data** Fig. 6d), suggesting that the discrepant tumor suppression by single-agent vs. combination L-fuc + anti-PD1 in our SW1 and SM1 mouse models (Fig. 5a) is attributed to determinants beyond the PD1:PD-L1 axis. Indeed, our global fucosylated and phosphoproteomic analyses suggests that fucosylation in $CD4^+$T cells impacts Integrin β5, PKA, and actin signaling (**Extended Data** Fig. 2), and that this is associated with increased intratumoral T cell presence and memory phenotypes in our models (Figs. 2 and 5)—consistent with previous reports that those functions are regulated by those pathways in T cell biology [15–17, 19]. That L-fuc can increase $CD4^+$T central memory cells also partially explains how it can augment anti-PD1 efficacy, which is associated with the presence of these cells [55]. How L-fuc may regulate these signaling pathways and enrich for $CD4^+$T memory subsets within the tumor microenvironment, and further, how L-fuc alters DC biology and induces their intratumoral accumulation (Figs. 2 and 5) may contribute to anti-tumor immune responses and tumor suppression in this context are unclear and warrant further lines of study. In addition, sex might be a determinant, as melanoma fucosylation levels are lower but correlate more strongly with intratumoral $CD3^+$T cells in male vs. female patients (Fig. 1j,k). Reduced melanoma fucosylation, which is expected to lower TILs, might explain increased lethality in male patients (American Cancer Society Facts & Figures, 2022).

The availability of pre-treatment anti-PD1 tumor tissue specimens for this study was extremely limited. Thus, the specimens that we acquired were subject to clinical variability that may have undermined statistical robustness in our analyses. Subsequent studies investigating tumor fucosylation,

total/fucosylated HLA-DRB1, and $CD4^+$T cells as biomarkers will need to factor for clinical variables including therapies received prior to anti-PD1, pre-existing medical conditions, as well as time from biopsy to anti-PD1 treatment. Since we were unable to control for these confounders in our specimens, it is unclear how they may have impacted tumor/HLA-DRB1 fucosylation and $CD4^+$T cell biology, and thus, the strength of correlations between these markers and responsiveness to treatment. Likewise, the importance and contribution of the immune environment of the peri-tumoral stroma in this setting remains to be elucidated, as some of our biopsies contained stroma, whereas other tumor core biopsies did not. Prior studies focusing on tumor:immune interactions and immunotherapies (including anti-PD1) have highlighted the importance of analyzing biomarker staining patterns at tumor:immune/tumor:stromal interfaces contained within biopsies, as these are areas of enriched immunological activity and signaling [63–65]. Lack of sufficient stroma among several biopsies likely significantly undermined statistical robustness of our trends/correlations. Indeed, we found that some specimens containing divergent tumor:stroma content did exhibit divergent correlation strengths (e.g., core biopsies containing only tumor vs. non-core biopsies containing significant stroma) For example, a “highly correlated” anti-PD1 responder (non-core biopsy) containing significant tumor:stromal interface exhibited correlated high levels of fucosylated HLA-DRB1 and $CD4^+$T cells, whereas a “non-correlated” responder (a core biopsy) did not (**Extended Data** Fig. 6e). The lack of stromal interface in the non-correlated responder biopsy is a likely explanation for lack of correlated levels of fuco-HLA-DRB1 and $CD4^+$T cells. The acquisition of such biopsy specimens that are controlled for the variables detailed above is an important consideration for subsequent studies. Our findings highlight the need for a prospective clinical trial with defined protocols for collection of mono-therapy anti-PD1 pre-treatment biopsies at defined timepoints proximal to therapy and clear biopsy protocols to yield tumor specimens that contain significant intact stromal interface.

In conclusion, fucosylation of HLA-DRB1 is a key regulator of TIL abundance in melanomas, and this mechanism, together with fucosylation-regulated $CD4^+$T cell biology, can be therapeutically exploited using oral L-fuc. Elucidation of the mechanistic determinants is expected to advance our understanding of the immunobiology of melanoma and other cancers and to inform efforts at implementing fucosylation/fucosylated HLA-DRB1 as biomarkers and of L-fuc as a therapeutic agent.

Methods

General cell culture

NHEM (normal adult epidermal melanocytes) were grown in Lonza MGM-4 growth media; prior to harvest for IB analysis, the cells were switched to the same media as the other cells overnight. WM793,1205Lu, A375, WM1366, WM164, and SW1 melanoma cells were obtained from the Ronai laboratory (Sanford-Burnham Prebys Medical Discovery Institute (La Jolla, CA), WM983A/B cells were purchased from Rockland Immunochemicals (Limerick, PA). WM115 and WM266-4 cells were purchased from ATCC (Manassas, VA). SM1 (Gift from the Smalley Laboratory at Moffitt), were cultured in Dulbecco's Modified

Eagle Medium containing 10% fetal bovine serum (FBS), 1 g/mL glucose, 4 mM L-glutamine in 37^{o}C in 5% CO_2. Cell lines were transfected using Lipofectamine 2000 (Invitrogen, Waltham, MA). Primary CD4 + T cells were harvested using the EasySep (StemCell Technologies) Human $CD4^+$ negative selection isolation kit (#17952) according to manufacturer's protocols.

Antibodies

The following antibodies were used as indicated: mouse anti-V5 (0.2 µg/mL Millipore Sigma (St. Louis, MO)), mouse anti-V5 gel (V5-10, Millipore Sigma (St. Louis, MO)), mouse anti-human HLA-DRB1 (0.2 µg/mL, IF, ab215835, Abcam (Cambridge, UK)), rabbit anti-human HLA-DRB1 (0.2 µg/mL WB, ab92371, Abcam (Cambridge, UK)), β-tubulin (0.3 µg/mL, E7, developed by M. McCutcheon and S. Carroll and obtained from Developmental Studies Hybridoma Bank (University of Iowa, Iowa City, IA)), goat anti-biotin (0.1 µg/mL Vector Labs (Burlingame, CA)), biotinylated AAL (0.4 µg/mL Vector Labs, Burlingame, CA), fluorescein-conjugated AAL (0.4 µg/mL Vector Laboratories, Burlingame, CA), Agarose UEA1 and AAL (Vector Laboratories, (Burlingame, CA)), anti-mouse CD4 (20 mg/kg, for immunodepletion, GK1.5, Bioxcell (West Lebanon, NH)), anti-mouse CD8 (20 mg/kg, for immunodepletion, 2.43, Bioxcell (West Lebanon, NH)), goat anti-mouse IgGκ horseradish peroxidase (HRP) (0.04 µg/mL, Santa Cruz Biotechnology (Dallas, TX)), mouse anti-rabbit HRP (0.04 µg/mL, Santa Cruz Biotechnology (Dallas, TX)), goat anti-rabbit AlexaFluor 488 (0.04 µg/mL, ThermoFisher Scientific (Waltham, MA)),), donkey anti-mouse AlexaFluor 594 (0.05 µg/mL, ThermoFisher Scientific (Waltham, MA)), AlexaFluor 594 donkey anti-rabbit (0.05 µg/mL, ThermoFisher Scientific (Waltham, MA)), rabbit anti-Mart1 (0.2 µg/mL, Millipore Sigma (St. Louis, MO), rabbit anti-S100 (0.2 µg/mL, Agilent Technologies (Santa Clara, CA)), APC anti-mouse CD3 (0.5 µg/mL, Biolegend (San Jose, CA)), Pacific Blue anti-mouse CD4 (0.5 µg/mL, BD Biosciences (San Jose, CA)), BV785 anti-mouse CD8 (0.5 µg/mL, BD Biosciences (San Jose, CA)), FITC anti-mouse F4/80 (0.5 µg/mL, BD Biosciences (San Jose, CA)), APC anti-mouse GR-1 (0.5 µg/mL, BD Biosciences (San Jose, CA)), PeCy7 anti-mouse CD11c (0.5 µg/mL, BD Biosciences (San Jose, CA)), PE anti-mouse NK1.1(0.5 µg/mL, BD Biosciences (San Jose, CA)), PE anti-mouse DX5 (0.5 µg/mL, BD Biosciences (San Jose, CA)), PerCP-Cy5.5 anti-mouse CD11b (0.5 µg/mL, BD Biosciences (San Jose, CA)), rabbit anti-human PD-L1 (clone #NBP1-76769; Noveus Biologicals, Centennial, CO), PE rat anti-mouse PD-L1 (clone #10F.9G2; (Biolegend, (San Diego, CA)), and phalloidin Alexafluor 488 (0.2µg/mL, ThermoFisher Scientific (Waltham, MA)), mouse anti-FLAG (0.2 µg/mL, clone M2, Millipore Sigma (St. Louis, MO)), rabbit anti-HLA-A (0.2 µg/mL, Proteintech (Rosemont, IL)), normal mouse IgG (Santa Cruz Biotechnology (Dallas, TX)), rabbit anti-KDEL (0.1 µg/mL, ThermoFisher Scientific (Waltham, MA)), mouse anti-PD1 (for *in vivo* studies, 20 mg/kg, clone# RMP1-14 Bioxcell (West Lebanon, NH)), donkey anti-goat plus PLA secondary antibody (Millipore Sigma (St. Louis, MO)), donkey anti-mouse plus PLA secondary antibody (Millipore Sigma (St. Louis, MO)), rat anti-mouse CD8 antibody (0.2 µg/mL, ThermoFisher Scientific (Waltham, MA)), AlexaFluor 594 goat anti-rat secondary antibody (0.05 µg/mL, ThermoFisher Scientific (Waltham, MA)), anti-CD3 (0.2 µg/mL, Clone PS1, Santa Cruz Biotechnology (Dallas, TX), PE anti-pan-MHC-I (HLA-A,B,C) (BD Pharmingen (San Jose, CA), FITC anti-pan-MHC-II (HLA-DP, DQ, DQ)(BD Pharmingen (San Jose,

CA), PerPCy5.5 anti-CD45 (Invitrogen (Waltham, MA)), APC anti-CD90 (Biolegend (San Diego, CA)), and BV421 anti EpCAM (Biolegend (San Diego, CA)).

Cloning and mutagenesis

Mouse fucokinase (mFuk) was cloned using cDNA from SW1 cells into pLenti-C-Myc-DDK-IRES-Puro expression vector (Origene Technologies (Rockville, MD)) into BAMHI and NHEI restriction sites. Mouse EB1 constructs was cloned using cDNA from SW1 cells into pLenti-C-Myc-DDK-IRES-Puro expression vector (Origene Technologies (Rockville, MD)) into ASCI and XHOI restriction sites. pLKO Non-targeting shRNA (shNT), pLKO shK1-1, pLKO shK1-2, pLKO shEB1-1, and pLKO shEB1-2 were obtained from Millapore Sigma (St. Louis). pLX304::EV was obtained from Origene Technologies (Rockville, MD). pLX304::HLA-A and pLX304::HLA-DRB1 constructs were obtained from DNAasu (PMID:21706014). HLA-DRB1 N48G and T129A as well as EB1 N46G mutants were generated using QuikChange II XL site-directed mutagenesis kit according to the manufacturer's protocol (Agilent Technologies (Santa Clara, CA)).

Proteomic mass spectrometric profiling of fucosylated proteins

WM793 cells stably transduced with pLenti-GFP empty vector (EV), pLenti-FUK-GFP, or shFUK were grown in triplicate to ~ 30–40% confluence in (3 x 15 cm^3 plates each). The cells were further cultured in the presence of 50μM L-fucose-alkyne for ~ 72 h to ~ 80% confluence. The cells were lysed in 1.5% N-dodecyl-beta-D-maltoside/20mM HEPES pH 7.4/protease and phosphatase inhibitors. Lysates were sonicated and cleared by centrifugation at full speed for 5 min at 4C. Lysates were acetone precipitated overnight. The pelleted proteins were resuspended and subjected to click-chemistry labeling with biotin-azide using the Click-It kit per manufacturer's protocol (Invitrogen). For negative control, pLenti-GFP-EV cells were not labeled with L-fucose-alkyne but were lysed, pelleted, and click-reacted with biotin-azide. All biotin-azide (biotinylated-fucosylated) samples were pulled down using neutravidin beads that were pre-blocked with 2% IgG-free BSA. Samples were submitted to the Sanford-Burnham Prebys proteomics core facility for on-bead digest; supernatants from on-bead digest were analyzed by LC/MS/MS. Hits that were increased by > 1.5 fold in pLenti-FUK-GFP-expressing cells and unchanged or decreased in pLenti-EV-GFP-expressing cells or decreased in pLenti-shFUK-expressing cells. Hits were subjected to Ingenuity Pathway Analysis (Qiagen).

Lectin pulldown

Control beads and AAL or UEA1 lectin-conjugated agarose beads were pre-blocked for 2 h in blocking buffer (2% IgG-Free BSA (Jackson ImmunoResearch Laboratories (Westgrove, PA)) on a rotator at 4^oC. Cells were lysed on ice in 1% Triton-X100 lysis buffer (1% Triton-X100, 20mM Tris-HCl, pH 7.4, 150mM NaCl in ddH2O + protease and phosphatase inhibitors (ThermoFisher Scientific (Waltham, MA)), briefly sonicated, pelleted, and the resulting lysates were normalized in protein concentration to the sample with the lowest concentration and diluted to a final 0.25% Triton-X-100 with dilution buffer (0% Triton X-100, 20mM Tris-HCl, pH 7.4, 150mM NaCl in ddH_2O + protease and phosphatase inhibitors (ThermoFisher

Scientific (Waltham, MA)), and incubated with 15µl of pre-blocked beads (beads were spun out of block and resuspended in dilution buffer) and rotated overnight at 4^{o}C. Next, the beads were washed twice with dilution buffer and subjected to (12%) SDS-PAGE and IB analysis using the indicated antibodies.

Mass spectrometric analysis of glycosylation on HLA-DRB1

Stained bands of approximately 1ug of exogenously expressed V5-HLA-DRB1 purified from WM793 cells were cut into 1-mm^3 pieces and reduced and alkylated using 20mM TCEP (tris(2-carboxyehtyl)phosphine) and iodoacetamide in 50mM Tris-HCl. The gel pieces were washed in a 20mM ammonium phosphate solution with 50% methanol overnight at 4°C. The following day, the gel pieces were dehydrated for 30 minutes with 100% acetonitrile. After gel pieces were completely dry, trypsin protease solution was added to the samples (300ng trypsin). Samples were digested for 4 hours at 37°C. The digests were applied to a C-18 Zip-Tip and eluted with 50% methanol and 0.1% formic acid. Five microliters of the elution were diluted in 0.1% formic acid and then injected into a Q-Exactive Orbitrap mass spectrometer (ThermoFisher Scientific, (Waltham, MA)) equipped with an Easy nano-LC HPLC system with reverse-phase column (ThermoFisher Scientific, (Waltham, MA)). A binary gradient solvent system consisting of 0.1% formic acid in water (solvent A) an 90% acetonitrile and 0.1% formic acid in water (solvent B) was used to separate peptides. Raw data files were analyzed using both Proteome Discoverer v2.1 (ThermoFisher Scientific, (Waltham, MA)) with Byonic (Protein Metrics) as a module and Byonic standalone v2.10.5. All extracted ion chromatograms (EICs) were generated using Xcalibur Qual Browser v4.0 (ThermoFisher Scientific, (Waltham, MA)). UniProt sequence Q5Y7D1_Human was used as the reference sequence for peptide analysis.

Phosphoproteomics mass spectrometric profiling of CD4 $^{+}$ T cells

CD4^{+}T cells cultured and treated as indicated in the main text were harvested and lysed in standard RIPA buffer + protease and phosphatase inhibitors. Protein concentration was estimated by BCA assay (Bio-Rad) and 1 mg lysates were subjected to trypsin digestion. Briefly, lysates were reduced with 4.5 mM dithiothreitol (DTT) for 30 min at 60^{0}C, alkylated with 10mM iodoacetamide (IAA) at room temperature in the dark for 20 minutes, and digested overnight at 37^{0}C with 1:20 enzyme-to-protein ratio of trypsin (Worthington). The resulting peptide solution was de-salted using reversed-phase Sep-Pak C_{18} cartridge (Waters) and lyophilized for 48 hours.

Fuco-proteomic mass spectrometric profiling of CD4 $^{+}$ T cells

CD4^{+}T cells cultured and treated as indicated in the main text were harvested, lysed in standard RIPA buffer + protease and phosphatase inhibitors, and subjected to lectin pulldown using control or AAL beads as described above. The beads were washed with PBS and subjected to on-bead trypsin digestion. Proteins bound to beads were denatured with 30mM ammonium bicarbonate at 95^{0}C for 5 minutes. Samples were reduced with 4.5 mM dithiothreitol (DTT) for 30 min at 60^{0}C, alkylated with 10mM iodoacetamide (IAA) at room temperature in the dark for 20 minutes, and digested overnight at 37^{0}C with

1:20 enzyme-to-protein ratio of trypsin (Worthington). The resulting peptide solution was acidified with a final concentration of 1% TFA. Samples were centrifuged at high speed and the supernatants were subjected to Ziptip purification (Millipore Ziptips, #Z720070). The eluted peptides were concentrated in a SpeedVac and suspended in 15 µL loading buffer (5% ACN and 0.1% TFA) prior to auto sampling. Samples were then subjected to LC-MS/MS as described below

Mass spectrometric identification of WT vs. glycofucomutant HLA-DRB1 interactors

V5-tagged WT or N48G glycofucomutant HLA-DRB1-expressing WM793 cells were lysed and subjected to V5 bead pulldown. Five percent of pulled down protein was immunblotted to ensure for equal sample submission for LC-MS/MS (**Extended Data Fig. 5a**). Samples were then subjected to LC-MS/MS as described below.

Liquid chromatography-MS/MS

On-bead digestion was performed with trypsin and tryptic peptides were then analyzed using a nanoflow ultra-high-performance liquid chromatograph (RSLC, Dionex, Sunnyvale, CA) coupled to an electrospray orbitrap mass spectrometer (Q-Exactive Plus, Thermo, San Jose, CA) for tandem mass spectrometry peptide sequencing. The peptide mixtures were loaded onto a pre-column (2 cm x 100 µm ID packed with C18 reversed-phase resin, 5µm, 100Å) and washed for 5 minutes with aqueous 2% acetonitrile and 0.1% formic acid. The trapped peptides were eluted and separated on a 75 µm ID × 50 cm, 2 µm, 100Å, C18 analytical column (Dionex, Sunnyvale, CA) using a 90-minute program at a flow rate of 300 nL/min of 2–3% solvent B over 5 minutes, 3 to 30% solvent B over 27 minutes, then 30–38.5% solvent B over 5 minutes, 38.5–90% solvent B over 3 minutes, then held at 90% for 3 minutes, followed by 90–2% solvent B in 1 minute and re-equilibrated for 18 minutes. Solvent A was composed of 98% ddH_2O and 2% acetonitrile containing 0.1% FA. Solvent B was 90% acetonitrile and 10% ddH_2O containing 0.1% FA. MS resolution was set at 70,000 and MS/MS resolution was set at 17,500 with max IT of 50 ms. The top sixteen tandem mass spectra were collected using data-dependent acquisition (DDA) following each survey scan. MS and MS/MS scans were performed in an Orbitrap for accurate mass measurement using 60 second exclusion for previously sampled peptide peaks. MaxQuant [66] software (version 1.6.2.10) was used to identify and quantify the proteins for the DDA runs.

PyMOL structural modeling

In **Fig. 4a**, structural modeling was performed using PyMOL (Molecular Graphics System, Version 2.0 Schrödinger, LLC) of the HLA-DRB1:HLA-DM complex (PDB ID, 4FQX); HLA-DRB1 (yellow) and DM (gray). For the CD4:HLA-DRB1:TCR complex, the model was reconstituted by superimposing the DRB1 beta chains from CD4:HLA-DR1 complex (PDB ID, 3S5L) and TCR:HLA-DR1 complex (PDB ID, 6CQR) using PyMOL. RMSD between the 163 backbone atoms is 0.497. The potential glycosylation sites, N48 and T129, of HLA-DR1 beta chain are shown as sticks. CD4 (cyan), HLA-DRB1 (yellow), antigen peptide (magenta), and TCR (green)(*lower right*).

TIL isolation protocol

Tumors of SW1 or SM1 melanoma cells from C3H/HeJ or C57BL/6 mice, respectively) were digested using 1X tumor digest buffer (0.5 mg/mL Collagenase I, 0.5 mg/mL Collagenase IV, 0.25 mg/mL Hyalyronidase V, 0.1 mg/ mL DNAse I in HBSS (Millipore Sigma (St. Louis, MO)). Tumors were homogenized using the Miltenyi MACs dissociator. Red blood cells were lysed using ACK lysis buffer (Life Technologies, (Grand Island, NY)). Tumor homogenate cells were counted using a standard hemocytometer.

Human donor peripheral $CD4^+$ T cell isolation protocol

Human $CD4^+$ T cells were isolated from fresh peripheral blood monocyte cells (PBMC) using a $CD4^+$ T cell negative selection isolation kit (Stem Cell Technologies, (Vancouver CA)) according to manufacturer's protocols. $CD4^+$ T cells were cultured in the presence of vehicle or 250μM L-fucose and were activated using anti-CD3/CD28 Dynabeads (ThermoFisher Scientific (Waltham, MA)) in a 1:1 bead:$CD4^+$ T cell ratio. After 48 h, cell pellets were collected and lysed for either lectin-based fucoproteomics or phosphoproteomics.

Flow Cytometry

Gating schemes can be found in the Supplementary Information

• itIC and splenic profiling:

Total TILs were gated first to single cells (based on forward scatter height vs width, followed by side scatter height vs. width). Live cells were gated from the Zombie negative population from the population above. TILs were gated based on splenocyte size from a control spleen. Individual immune subpopulations were sub-gated from the total TIL population using the following staining criteria: $CD3^+$ for $CD3^+$ T cells; $CD3^+/CD4^+/CD8^-$ for CD4 + T cells; $CD3^+/CD4^-/CD8^+$ for $CD8^+$ T cells, $CD11c^+/CD11b^+$ for DCs; either NK1.1 (for C57/BL6 mice) or DX5 (for C3H/HeJ) for NK cells; $CD11b^+/GR1^+$ for MDSC-like cells; and $F4/80^+$ for macrophages. Single-cell suspensions from tumor and spleen tissue were stained with Live/Dead Zombie NIR (Biolegend, (San Diego, CA)) at 1:1,000 in PBS for 20 min. Cell suspensions were spun down and stained with the following with antibodies at 0.5 μg/ml per antibody: APC anti-mouse CD3, Pacific Blue anti-mouse CD4, BV785 anti-mouse CD8, PerCP anti-mouse CD25, FITC anti-mouse F4/80, PeCy7 anti-mouse CD11c, PE anti-mouse NK1.1 or PE anti-mouse DX5, and PerCP-Cy5.5 anti-mouse CD11b. After staining, the cells were washed and fixed (2% formaldehyde), followed by another wash and flow cytometric analysis. The compensation controls were prepared using 0.5 μg/mL of each antibody with UltraComp eBeads, (ThermoFisher Scientific (Waltham, MA)). All samples were subject to flow cytometric profiling using a LSR Flow Cytometer (BD Biosciences (San Jose, CA)) and analysis as indicated using FlowJo software (BD Biosciences (San Jose, CA)).

• Assessment of cell surface fucosylation, HLA-DRB1, and PD-L1: Indicated cells were treated for 72 h with DMSO, 250 μM fucosyltransferase inhibitor (FUTi) (Millipore Sigma (St. Louis, MO)), or 250 μM of L-fucose (Biosynth (Oak Terrace, IL)). After 72 h, cells were stained with 0.1 μM PKH26 (Millipore Sigma (St. Louis, MO)) prior to fixation in 4% formaldehyde solution. The cells were stained with anti-HLA-DRB1 and fluorescein AAL, or anti-human or anti-mouse PD-L1 overnight. The following day the cells were washed 3 times prior to adding AlexaFluor 594 donkey anti-rabbit. Cells were washed 3 times and then subject to flow cytometric analyses using a FACSCalibur (BD Biosciences (San Jose, CA)). Samples were analyzed using FlowJo analysis software (BD Biosciences (San Jose, CA)). Median values of DRB1 and AAL were normalized to PKH26 values and statistical analysis was performed using GraphPad Prism.

• Assessment of cell surface pan-MHC-I and pan-MHC-II: Surgically resected patient tumors were minced to less than 1-mm fragments. Minced tumor sample was enzymatically digested in enzyme media comprised of RPMI with collagenase type IV (1 mg/mL), DNase type IV (30 U/mL), and hyaluronidase type V (100 μg/mL) (Sigma). Single cell suspensions were strained through 40-micron nylon mesh and counted for viability via trypan blue exclusion, followed by cryopreservation for future analysis. Tumor homogenates were thawed and stained using Live / Dead Zombie NIR, PE anti-pan-MHC-I (HLA-A,B,C), FITC anti-pan-MHC-II, PerPCy5.5 anti-CD45, APC anti-CD90, and BV421 anti EpCAM. Flow cytometric data was analyzed using FlowJo analysis software (BD Biosciences (San Jose, CA)). MHC-I and MHC-II expression was dichotomized as positive or negative based on FMO samples for each marker. Statistical analysis was performed using GraphPad Prism.

Immunoprecipitation and immunoblot analyses

Cells were lysed on ice in RIPA lysis buffer (25 mM Tris-HCl pH 7.6, 150 mM NaCl, 5 mM EDTA, 1% NP-40 or 1% Triton X-100, 1% sodium deoxycholate, 0.1% SDS in diH_20 + protease and phosphatase inhibitors (ThermoFisher Scientific (Waltham, MA)), briefly sonicated, pelleted, and the resulting lysates were normalized by protein concentration using DC assay (BioRad Laboratories, (Hercules, CA)). The indicated samples were subjected to (12%) SDS-PAGE and immunoblot analysis using the indicated antibodies. Immunoblot imaging and analysis was performed using either an Odyssey FC scanner and ImageStudio (LiCor Biosciences, Lincoln, NE) or film.

qRT-PCR

RNA from cells subjected to the indicated treatments was extracted using Gene Elute Mammalian Total RNA Extraction System (Millipore Sigma (St. Louis, MO)). RNA was reversed transcribed to cDNA using High-Capacity cDNA Reverse Transcription Kit (ThermoFisher Scientific (Waltham, MA)). qRT-PCR analysis was performed using FastStart Universal SYBR Green Master Mix (Rox) (Roche Diagnostics, (Indianapolis, IN)) using a BioRad CFX96 Real-time system (BioRad Laboratories, (Hercules, CA)). The qRT-PCR cycles used were as follows: 95°C for 10 min, 35 cycles of 95°C for 15 seconds, 55°C for 60 seconds, and 72°C for 30 seconds. Expression of the indicated genes was normalized to histone H3A

expression. Primers for qRT-PCR were generated using NCBI primer blast software (National Center for Biotechnology Information (Washington, D.C.)) as detailed the table below.

Primer	Sequence (5’ -> 3’)
Cloning Primers	_
Fuk (mouse)	F: cgcgcgcgGGATCCatggagcagtcagagggagtcaattggactg
	R: cgcgcgcgGCTAGCggtggtgcccacttcagagggcc
HLA-DRB1 N48G	F: GTCTTTGAAGGATACACAGCCACCTTAGGATGGACTCG
	R: tgagtgtcatttcttcggtgggacggagcggg
HLA-DRB1 T129A	F: CGAGTCCATCCTAAGGTGGCTGTGTATCCTTCAAAGAC
	R: GTCTTTGAAGGATACACAGCCACCTTAGGATGGACTCG
EB1	F: cgcgcccgGGCGCGCCatggtggtgtggc
	R: cgcgcccgCTCGAGgctcaggagtcc
EB1 N46G	F: GTGTCATTTCTACGGCGGGACGCAGCGC
	R: GCGCTGCGTCCCGCCGTAGAAATGACAC
qRT-PCR	_
H3A (human and mouse)	F: AAGCAGACTGCCGCAAAT
	R: GGCCTGTAACGATGAGGTTTC
Fuk (mouse)	F: ACTTCCGCCGAGATCTGTTC
	R: GGATCAGTGGACGTAGGCAG
EB1	F: GAACACGCTTCTTCCTTGGG
	R: CAGGCTCCTTACCTTTCTGGT
H2-K1	F: CCGCGGACGCTGGATA
	R: GGCGATTCGCGACTTCTG
HLA-DRB1	F: CCATAGTAGCTCAGCACCCG
	R: GTCCTGTCCTGTTCTCCAGC

Fluorescent immunocytochemical and immunohistological staining and analysis

• General fluorescent immunocytochemical staining protocol: Melanoma cells were grown on German glass coverslips (Electron Microscopy Services (Hatfield, PA)) and fixed in fixation buffer (4%

formaldehyde, 2% sucrose in phosphate buffered saline (PBS) for 20 min at room temperature (RT). The coverslip-grown cells were subject to two 5-min standing washes in PBS prior to permeabilization in permeabilization buffer (0.4% Triton-X-100 and 0.4% IgG-free bovine serum albumin (BSA, Jackson ImmunoResearch Laboratories (Westgrove, PA) in PBS) for 20 min at RT. The coverslip-grown cells were next subject to 2 PBS washes and incubated with the indicated primary antibodies.

• General fluorescent immunohistochemical tissue staining protocol: In general, paraffin-embedded FFPE tumor tissue sections (or the TMA slide) were melted at 70°C for 30 min. The slides were further de-paraffinizeded using xylene and rehydrated in serial alcohol washes. The slides were pressure cooked at 15 PSI for 15 min in a 1X DAKO antigen retrieval buffer (Agilent Technologies (Santa Clara, CA)). The tumor sections were subject to two 5-min standing washes in PBS prior to blocking in 1X Carb-Free Blocking Solution (Vector Labs (Burlingame, CA)) for 2-3h. The slides were next washed twice and incubated with indicated lectin and/or antibodies.

General fluorescent analysis of mouse tumor tissue fucosylation (Extended Data Figs. 1a,d,k):

For assessment of mouse tumor fucosylation, FFPE tumor sections were immunostained with FITC-conjugated AAL lectin (0.4 µg/mL, Vector Laboratories (Burlingame, CA)) and rabbit anti-Mart1 + rabbit anti-S100 (melanoma marker cocktail). The slides were mounted with Vectashield + DAPI (Vector Laboratories (Burlingame, CA)). Four representative microscopy images per tumor were acquired using a Keyence BZ-X710, and images were process and analyzed using FIJI (NIH) as follows: melanoma marker-positive regions were assigned as regions of interest (ROI) in which we measured Integrated density of AAL signal. Integrated densities of control tumors were assigned as 1, and Integrated AAL density values of experimental tumors were divided by control to produce relative fold changes and plotted as column charts.

• Immunofluorescent staining and analysis of melanoma tissues and TMA (Fig. 1N):

Immunostaining and image acquisition: Melanoma TMA (Serial #ME1002b; US BioMax, Inc. (Derwood, MD)) was immunostained with FITC-conjugated AAL lectin (0.4 µg/mL, Vector Laboratories (Burlingame, CA)), rabbit anti-Mart1, rabbit anti-S100, and anti-CD3 followed by AlexaFluor 568 (Cy3) donkey anti-rabbit and AlexaFluor 647 (Cy5) donkey anti-mouse secondary antibodies. The slides were mounted with Vectashield + DAPI (Vector Laboratories (Burlingame, CA)). An Aperio Scanscope FL (Leica Biosystems) was used to scan the TMA slide at 20X magnification and the digital slide saved into the Spectrum e-slide database.

Analysis: The multiplex fluorescence TMA image file was imported into Definiens Tissue Studio version 4.7 (Definiens AG, Munich, Germany), where individual cores were identified using the software's automated TMA segmentation tool. First, nucleus segmentation (DAPI channel) and cell growth algorithms were used to segment individual cells within each core. A minimum size threshold was used to refine the cell segmentation. Next, mean fluorescence intensity (MFI) values for the FITC (fucosylation), Cy3 (melanoma markers Mart1 + S100) and Cy5 (CD3 marker) channels were extracted

from each segmented cell and minimum thresholds for MFI was set to enumerate positive Cy3 and Cy5 cells. Identical thresholds were used for each core. Finally average MFI values for each core were reported for the FITC and Cy3 channels.

Melanoma-specific fucosylation (FITC in CY3-positive cells) MFI and $CD3^+$ cell numbers were subject to statistical analyses and correlation with clinical parameters as follows: We used the nonparametric Wilcoxon rank sum test to compare melanoma-specific fucosylation levels between $CD3^+$ T cells high vs low groups. The density values of $CD3^+$ T cells were all log2 transformed in the statistical analysis. Multivariable linear regression was used to assess the association between fucosylation and T cells while adjusting for confounding factors including sex, age and stage. The Spearman correlation coefficient was used to measure the correlation between melanoma-specific fucosylation and T cells in different sex groups.

Lectin-mediated proximity ligation assay (L-PLA)

Coverslip-grown cells subjected to L-PLA were processed upfront as described in the fluorescent immunocytochemistry protocol detailed above, whereas FFPE tumor tissue sections were processed according to the fluorescent immunohistochemistry protocol detailed above. Both approaches used mouse-anti-HLA-DRB1 (applied at 0.2 µg/mL, ab215835, Abcam, Cambridge, UK), biotinylated AAL lectin (applied at 0.2 µg/mL, Vector Laboratories (Burlingame, CA)), on coverslips overnight in 4^oC. The coverslip-grown cells were again washed twice with PBS followed and then incubated with phalloidin Alexafluor 488 (applied at 0.05 µg/mL, ThermoFisher Scientific (Waltham, MA) with goat anti-biotin (applied at 0.1 µg/mL, Vector Laboratories (Burlingame, CA)) for 2h in 4^oC. Subsequent steps of the protocol were adapted from the DUOlink In Situ Green PLA kit's manufacturer's protocol (Millipore Sigma (St. Louis, MO)). PLA anti-goat MINUS and PLA anti-mouse PLUS probes were applied at 1:5 for 1 h at 37^oC. The coverslips were washed twice with Wash Buffer A prior to ligation with 1:5 ligation buffer and 1:40 ligase in ddH2O for 30 min at 37^oC. The coverslips were washed twice with wash buffer A prior to incubation in amplification mix (1:5 amplification buffer and 1:80 polymerase in ddH2O for 1.5 h at 37^oC). Coverslips were washed twice with Wash Buffer B prior to mounting to slide with DAPI with VectaShield (Vector Labs, Burlingame, CA). Microscopy images were acquired using a Keyence BZ-X710, and images were process and analyzed using FIJI (NIH).

• Immunofluorescent staining, image acquisition, and analysis of anti-PD1-treated melanoma patients (FIG. 5c):

The indicated FFPE sections were immunostained with anti-DRB1 antibody or L-PLA stained as detailed above with the addition of anti-$CD4^+$ antibody. WTS imaging was performed using the Vectra3 Automated Quantitative Pathology Imaging System (PerkinElmer, Waltham, MA). 20X ROI tiles were sequentially scanned across the slide and spectrally unmixed using InForm (PerkinElmer, Waltham, MA) and the multilayer Tiff files were exported. HALO (indica labs, Albuquerque, NM) was used to fuse the tile images together prior to WTS image analysis. For each whole tumor image, (i) every individual melanoma

marker (MART1 + S100)-positive cell was segmented and quantitatively measured for total fucosylation, total HLA-DRB1, and fucosylated HLA-DRB1, and (ii) every $CD4^+$T cell within the melanoma marker-positive tissue region was counted. Per patient (Pt.), these marker values were box plotted to visualize the staining distribution of individual tumor cells. The total numbers of melanoma cells per patient section measured and analyzed were as follows: Pt. 1: 557,146 cells; Pt. 2: 743,172 cells; Pt. 3: 95,628 cells; and Pt. 4: 13,423 cells.

Anti-PD1-treated patient specimens (FIGs. 5d & 5e, and EXTENDED DATA FIGs. 4D & 4E)

Moffitt Cancer Center patient specimens: Patients with advanced stage melanoma being treated at Moffitt Cancer Center were identified, and specimens collected and analyzed following patient consent under Moffitt Cancer Center Institutional Review Board approved protocols.

• For FIGs. 5d & 5e: De-identified Moffitt “Responder” patients exhibited greater than 20 months of progression-free survival, whereas “Non-Responder” patients progressed in less than 6 months after receiving anti-PD1.

• For Extended Data FIGs 4D & 4E: Non-response status to PD1 checkpoint blockade therapy (nivolumab or pembrolizumab) was defined as progression of disease by RECIST 1.1 while on PD-1 checkpoint blockade therapy or within 3 months of last dose.

MD Anderson Cancer Center patient specimens: Biospecimens were retrieved, collected and analyzed after patient consent under UT MD Anderson Cancer Center Institutional Review Board-approved protocols. Patients with advanced (stage III/IV) melanoma treated at The University of Texas MD Anderson Cancer Center between 07/01/2015 and 05/01/2020 who received at least one dose of PD-1 checkpoint blockade agent (either nivolumab or pembrolizumab) were identified from detailed retrospective and prospective review of clinic records. Responder status was defined as a complete or partial response and non-responder was defined as stable or progressive disease by RECIST 1.1. Pathologic response was defined by the presence or absence of viable tumor on pathologic review when available.

Massachusetts General Hospital patient specimens: Patients initiating anti-PD1 (Pembrolizumab) as front-line treatment for metastatic melanoma at MGH provided written informed consent for the collection of tissue and blood samples for research and genomic profiling (DF/HCC IRB approved Protocol 11–181). Patients classified as responders (R) showed clear radiographic decrease in disease at initial staging through a minimum of 12 weeks. Patients classified as non-responders (NR) did not respond to treatment radiographically and/or had clear and rapid progression. Progression free survival (PFS) is given in days from treatment start to radiographic scan when progression was first noted (uncensored) or last progression free scan (censured). Overall survival (OS) is given in days from treatment start to date of death (uncensored) or last follow-up (censored).

Animal models

All animals were housed at the Vincent A. Stabile Research building animal facility at H. Lee Moffitt Cancer Center & Research Institute, which is fully accredited by the Association for Assessment and Accreditation of Laboratory Animal Care International (AAALAC, #434), and are managed in accordance with the Guide for the Care and Use of Laboratory Animals ("The Guide"), the Animal Welfare Regulations Title 9 Code of Federal Regulations Subchapter A, "Animal Welfare", Parts 1–3 (AWR), the Public Health Service Policy on Humane Care and Use of Laboratory Animals (PHS Policy), and by the USF Institutional Animal Care and Use Committee's Principles and Procedures of Animal Care and Use (IACUC Principles). The experiments and protocols detailed in this study received institutional approval by the Moffitt IACUC (RIS00001625). Four-to-six-week-old female C3H/HeN and male C57BL6 mice were purchased from Charles Rivers Laboratories for the indicated experiments. Four-to-six-week-old male NSG mice from the Lau laboratory breeding colony were used for the indicated experiments. Power calculations were used to determine mouse cohort sizes to detect significant changes in tumor sizes. In general, 10 mice per indicated cohort to accommodate for incidental loss of mice due to issues beyond our control (*e.g.*, incidental tumor ulceration that required exclusion from the study). Mouse tumor volumes were measured using length, width and depth divided by 2. At each experimental endpoint, mice were humanely euthanized using CO_2 inhalation in accordance to the American Veterinary Medical Association guidelines. Mice were observed daily and humanely euthanized if the tumor reached 2,000 mm^3 or mice showed signs of metastatic disease.

For all mouse models, 1 x 10^6 melanoma cells were injected subcutaneously in the right hind flanks of each mouse. Between 7–14 days, when the tumor volumes reached ~ 150 mm^3, the mice were either supplemented with or without 100 mM L-fucose (Biosynth (Oak Terrace, IL)) *via* drinking water, which was provided *ad libitum* and which we previously demonstrated to increase tumor fucosylation and to suppress melanomas [8]. This dosage is within previously reported ranges for dietary supplementation with L-fucose and other similar dietary sugars (e.g., D-mannose) in other rodent studies [67–71]. When the tumors reached ~ 2 cm^3, the animals were sacrificed, and the tumors either processed for flow cytometric profiling or for histological analysis as indicated.

• Control vs. mFuk ± L-fucose models (Fig. 1 & Extended Data Fig. 1): SW1 or SM1 mouse melanoma cells were injected into syngeneic C3H/HeN (or NSG) female or C57BL/6 male mice, respectively, as follows: parental SW1 cells for **Fig. 1A**; parental SM1 cells for **Fig. 1E**; SW1 cells stably expressing either empty vector (EV) or mouse fucose kinase (mFuk) for **Fig. 1L**; and parental SW1 cells for **Fig. 1M**.

• Control vs. L-fucose ± FTY720 models (Fig. 2): SW1 or SM1 mouse melanoma cells were injected into syngeneic C3H/HeN (or NSG) female or C57BL/6 male mice, respectively. Cells were injected as follows: parental SW1 cells for **Fig. 1A**; parental SM1 cells for **Fig. 1E**; SW1 cells stably expressing either empty vector (EV) or mouse fucose kinase (mFuk) for **Fig. 1L**; and parental SW1 cells for **Fig. 1M**. FTY720 was administered at 20 µg every 2 days starting on Day 12, just prior to the initiation of LF, until endpoint.

• Immunodepletion mouse models (Fig. 1 & Extended Data Fig. 1): Three days prior to tumor engraftment, PBS (control) or ~ 300 µg α-CD4 (20 mg/kg, for immunodepletion, GK1.5, Bioxcell (West Lebanon, NH)) or

α-CD8 (20 mg/kg, for immunodepletion, 2.43, Bioxcell (West Lebanon, NH)) was administered by intraperitoneal injection into the indicated cohorts of mice. Injections of immunodepletion antibody or PBS were continued every 3–4 days until endpoint. Syngeneic recipient C3H/HeN female or C57BL/6 male mice were injected with SW1 or SM1 cells, respectively.

• HLA-A/HLA-DRB1 knockdown and glyco-fucomutant H2-EB1 reconstitution mouse model (Figs. 2 & 3): SW1 mouse melanoma cells expressing either shNT (non-targeting shRNA), shH2K1, shEB1, shNT + EV, shEB1 + EV, shEB1 + EB1 WT, or shEB1 + EB1 N46G were injected into syngeneic C3H/HeN female mice.

• anti-PD-1 mouse model (Figs. 4): SW1 or SM1 mouse melanoma cells were injected into syngeneic C3H/HeN female or C57BL/6 male mice, respectively. After approximately 7 days, when the mice tumors reached ~ 150 mm^3, the mice were either supplemented with or without 100 mM L-fucose (Biosynth (Oak Terrace, IL)) *via* drinking water, which was provided *ad libitum*. Simultaneously, PBS (control) or anti-PD1 (20 mg/kg, clone RMP1-14, Bioxcell (West Lebanon, NH)) were administered via intraperitoneal injection every 3–4 days until endpoint. Mice were sacrificed, and tumors and indicated organs were harvested for analysis at indicated timepoints.

• NSG melanoma model (Fig. 1 model): SW1 murine mouse melanoma cells were subcutaneously injected into the right rear flanks of NSG mice.

Quantification and statistical analysis

GraphPad Prism was used for statistical calculations unless otherwise indicated. For all comparisons between 2 independent conditions, t tests were performed to obtain p values and standard error of the mean (SEM). For comparisons between ≥ 2 groups, one way or two-way ANOVAs were performed, and p values and SEMs were obtained. For the TMA data, Wilcoxon signed-rank test was used to determine significance.

Declarations

AUTHOR CONTRIBUTIONS

Conceptualization: E.L., D.K.L, S.A.P., V.L.; Methodologies: E.L., D.K.L., B.C., P.I., K.K., Q.L., E.A., D.B.W., M.B., A.M-M., M.M., G.W., C.MS., S.M., A.G., L.D., V.I.; Computational Analysis: Q.Q.M., D.B.W., B.C., J.J., J.N., X.W.; Resources: J.M., J.M., C.P.L, K.L.T., D.T.F., T.S., M.G.W., J.A.W., G.M.B., B.R.; Writing: E.L., D.K.L.; Supervision: E.L., S.A.P., V.L., R.S.H., X.W., B.R., J.M.K.; Funding Acquisition: E.L., R.S.H. All of the authors commented on the manuscript.

ACKNOWLEDGEMENTS

We are grateful to all Lau laboratory members and to Drs. Srikumar Chellappan, John Cleveland, José Conéjo-Garcia, Gina DeNicola, Florian Karreth, Ana Gomes, and Daniel Abate-Daga at Moffitt Cancer Center for critical readings of this manuscript. We would also like to thank Dr. Ze'ev Ronai for his

mentorship, as well as Drs. Michiko Fukuda, Minoru Fukuda, and Hudson Freeze for their technical advice and guidance in glycobiological studies. We would like to acknowledge to Dr. Eva Sahakian for technical assistance and advice and Ms. Melissa Meister, Theresa Alvarez, and Tara Christie for administrative support. This work has been supported in part by the Moffitt/USF Vivarium, Flow Cytometry Core, Biostatistics, Analytical Microscopy, Tissue Core Facilities (we would like to thank in particular Mr. Noel Clark and Ms. Jodi Balasi for technical support) and Advanced Analytical and Digital Laboratory at H. Lee Moffitt Cancer Center & Research Institute, an NCI designated Comprehensive Cancer Center (P30-CA076292). We would like to acknowledge the Proteomic Shared Resource of the Sanford Burnham Prebys Medical Discovery Institute for their assistance with the fucosylated proteomic screening. Support from a NIGMS grant (GM061126 to R.S.H.), NCI grants (K99CA172705, R00CA172705, and R01CA241559 to E.L.), a Harry J. Lloyd Charitable Trust Melanoma Research grant (to E.L.) are gratefully acknowledged.

COMPETING INTERESTS

G.M.B. has SRA with Palleon Pharmaceuticals, Olink Proteomics, InterVenn Biosciences, and formerly with Takeda Oncology. She consults for Merck and InterVenn. She served on SAB and a steering committee for Nektar Therapeutics. J.M. has served on an advisory board for Array Biopharma in the past 2 years and has been PI of grants/funding to his institution from Morphogenesis Inc, Navigate Biopharma, Jackson Labs, Microba, Merck, Macrogenics, and Reata Pharmaceuticals. Moffitt Cancer Center has licensed Intellectual Property (IP) related to the proliferation and expansion of tumor infiltrating lymphocytes (TILs) to Iovance Biotherapeutics. Moffitt has also licensed IP to Tuhura Biopharma. S.P.T. is an inventor on such Intellectual Property. S.P.T. is listed as a co-inventor on a patent application with Provectus Biopharmaceuticals. S.P.T. participates in sponsored research agreements with Provectus Biopharmaceuticals, Iovance Biotherapeutics, Intellia Therapeutics, Dyve Biosciences, and Turnstone Biologics that are not related to this research. S.P.T. has received ad hoc consulting fees from Seagen Inc. and serves as an advisor for KSQ Therapeutics.

DATA AVAILABILITY

The authors declare that the main data supporting the findings of this study are available within the article and its Supplementary Information files. Additional data are available from the corresponding author upon request.

References

1. Weber, J.S. *et al.* Nivolumab versus chemotherapy in patients with advanced melanoma who progressed after anti-CTLA-4 treatment (CheckMate 037): a randomised, controlled, open-label, phase 3 trial. *Lancet Oncol* **16**, 375-384 (2015).
2. Chacon, J.A. *et al.* Manipulating the tumor microenvironment ex vivo for enhanced expansion of tumor-infiltrating lymphocytes for adoptive cell therapy. *Clin Cancer Res* **21**, 611-621 (2015).

3. Spitzer, M.H. *et al.* Systemic Immunity Is Required for Effective Cancer Immunotherapy. *Cell* **168**, 487-502 e415 (2017).
4. Schneider, M., Al-Shareffi, E. & Haltiwanger, R.S. Biological functions of fucose in mammals. *Glycobiology* **27**, 601-618 (2017).
5. Marth, J.D. & Grewal, P.K. Mammalian glycosylation in immunity. *Nat Rev Immunol* **8**, 874-887 (2008).
6. Keeley, T.S., Yang, S. & Lau, E. The Diverse Contributions of Fucose Linkages in Cancer. *Cancers (Basel)* **11** (2019).
7. Adhikari, E. *et al.* L-fucose, a sugary regulator of antitumor immunity and immunotherapies. *Mol Carcinog* (2022).
8. Lau, E. *et al.* The transcription factor ATF2 promotes melanoma metastasis by suppressing protein fucosylation. *Sci Signal* **8**, ra124 (2015).
9. Yang, S. *et al.* Melanoma cells transfected to express CD83 induce antitumor immunity that can be increased by also engaging CD137. *Proc Natl Acad Sci U S A* **101**, 4990-4995 (2004).
10. Knight, D.A. *et al.* Host immunity contributes to the anti-melanoma activity of BRAF inhibitors. *J Clin Invest* **123**, 1371-1381 (2013).
11. Maletzki, C. *et al.* NSG mice as hosts for oncological precision medicine. *Lab Invest* **100**, 27-37 (2020).
12. Kennedy, R. & Celis, E. Multiple roles for CD4+ T cells in anti-tumor immune responses. *Immunol Rev* **222**, 129-144 (2008).
13. Lim, C.J. *et al.* Integrin-mediated protein kinase A activation at the leading edge of migrating cells. *Mol Biol Cell* **19**, 4930-4941 (2008).
14. Das, M., Ithychanda, S., Qin, J. & Plow, E.F. Mechanisms of talin-dependent integrin signaling and crosstalk. *Biochim Biophys Acta* **1838**, 579-588 (2014).
15. del Pozo, M.A., Sanchez-Mateos, P., Nieto, M. & Sanchez-Madrid, F. Chemokines regulate cellular polarization and adhesion receptor redistribution during lymphocyte interaction with endothelium and extracellular matrix. Involvement of cAMP signaling pathway. *J Cell Biol* **131**, 495-508 (1995).
16. Nordenfelt, P., Elliott, H.L. & Springer, T.A. Coordinated integrin activation by actin-dependent force during T-cell migration. *Nat Commun* **7**, 13119 (2016).
17. Kumari, S. *et al.* Cytoskeletal tension actively sustains the migratory T-cell synaptic contact. *EMBO J* **39**, e102783 (2020).
18. Zhi, L. *et al.* FTY720 blocks egress of T cells in part by abrogation of their adhesion on the lymph node sinus. *J Immunol* **187**, 2244-2251 (2011).
19. Oberprieler, N.G. *et al.* High-resolution mapping of prostaglandin E2-dependent signaling networks identifies a constitutively active PKA signaling node in CD8+CD45RO+ T cells. *Blood* **116**, 2253-2265 (2010).

20. Binnewies, M. *et al.* Unleashing Type-2 Dendritic Cells to Drive Protective Antitumor CD4(+) T Cell Immunity. *Cell* **177**, 556-571 e516 (2019).
21. Tay, R.E., Richardson, E.K. & Toh, H.C. Revisiting the role of CD4(+) T cells in cancer immunotherapy-new insights into old paradigms. *Cancer Gene Ther* **28**, 5-17 (2021).
22. Bajana, S. *et al.* Differential CD4(+) T-cell memory responses induced by two subsets of human monocyte-derived dendritic cells. *Immunology* **122**, 381-393 (2007).
23. Kramer, A., Green, J., Pollard, J., Jr. & Tugendreich, S. Causal analysis approaches in Ingenuity Pathway Analysis. *Bioinformatics* **30**, 523-530 (2014).
24. Rossjohn, J. *et al.* T cell antigen receptor recognition of antigen-presenting molecules. *Annu Rev Immunol* **33**, 169-200 (2015).
25. Rock, K.L., Reits, E. & Neefjes, J. Present Yourself! By MHC Class I and MHC Class II Molecules. *Trends Immunol* **37**, 724-737 (2016).
26. Orczyk-Pawilowicz, M., Augustyniak, D., Hirnle, L. & Katnik-Prastowska, I. Lectin-based analysis of fucose and sialic acid expressions on human amniotic IgA during normal pregnancy. *Glycoconj J* **30**, 599-608 (2013).
27. Bastian, K., Scott, E., Elliott, D.J. & Munkley, J. FUT8 Alpha-(1,6)-Fucosyltransferase in Cancer. *Int J Mol Sci* **22** (2021).
28. Hashim, O.H., Jayapalan, J.J. & Lee, C.S. Lectins: an effective tool for screening of potential cancer biomarkers. *PeerJ* **5**, e3784 (2017).
29. Nonaka, M. *et al.* Mannan-binding protein, a C-type serum lectin, recognizes primary colorectal carcinomas through tumor-associated Lewis glycans. *J Immunol* **192**, 1294-1301 (2014).
30. Osuga, T. *et al.* Relationship Between Increased Fucosylation and Metastatic Potential in Colorectal Cancer. *J Natl Cancer Inst* **108** (2016).
31. Zou, X. *et al.* A standardized method for lectin microarray-based tissue glycome mapping. *Sci Rep* **7**, 43560 (2017).
32. Yuhki, N. *et al.* Comparative genome organization of human, murine, and feline MHC class II region. *Genome Res* **13**, 1169-1179 (2003).
33. Rubio, G. *et al.* Cross-linking of MHC class I molecules on human NK cells inhibits NK cell function, segregates MHC I from the NK cell synapse, and induces intracellular phosphotyrosines. *J Leukoc Biol* **76**, 116-124 (2004).
34. Chang, C.S., Brossay, L., Kronenberg, M. & Kane, K.P. The murine nonclassical class I major histocompatibility complex-like CD1.1 molecule protects target cells from lymphokine-activated killer cell cytolysis. *J Exp Med* **189**, 483-491 (1999).
35. Raulet, D.H. *et al.* Specificity, tolerance and developmental regulation of natural killer cells defined by expression of class I-specific Ly49 receptors. *Immunol Rev* **155**, 41-52 (1997).
36. Gay, D. *et al.* Functional interaction between human T-cell protein CD4 and the major histocompatibility complex HLA-DR antigen. *Nature* **328**, 626-629 (1987).

37. Walser-Kuntz, D.R., Weyand, C.M., Fulbright, J.W., Moore, S.B. & Goronzy, J.J. HLA-DRB1 molecules and antigenic experience shape the repertoire of CD4 T cells. *Hum Immunol* **44**, 203-209 (1995).
38. Fleury, S. *et al.* HLA-DR polymorphism affects the interaction with CD4. *J Exp Med* **182**, 733-741 (1995).
39. Steentoft, C. *et al.* Precision mapping of the human O-GalNAc glycoproteome through SimpleCell technology. *EMBO J* **32**, 1478-1488 (2013).
40. Stern, L.J. *et al.* Crystal structure of the human class II MHC protein HLA-DR1 complexed with an influenza virus peptide. *Nature* **368**, 215-221 (1994).
41. Pandey, A. *et al.* Glycosylation of Specific Notch EGF Repeats by O-Fut1 and Fringe Regulates Notch Signaling in Drosophila. *Cell Rep* **29**, 2054-2066 e2056 (2019).
42. Lenertz, L.Y. *et al.* Mutation of putative N-linked glycosylation sites on the human nucleotide receptor P2X7 reveals a key residue important for receptor function. *Biochemistry* **49**, 4611-4619 (2010).
43. Tsiakas, K. *et al.* Mutation of the glycosylated asparagine residue 286 in human CLN2 protein results in loss of enzymatic activity. *Glycobiology* **14**, 1C-5C (2004).
44. Wei, W. *et al.* Molecular mechanisms of missense mutations that generate ectopic N-glycosylation sites in coagulation factor VIII. *Biochem J* **475**, 873-886 (2018).
45. Rillahan, C.D. *et al.* Global metabolic inhibitors of sialyl- and fucosyltransferases remodel the glycome. *Nat Chem Biol* **8**, 661-668 (2012).
46. Anderson, K.S. & Cresswell, P. A role for calnexin (IP90) in the assembly of class II MHC molecules. *EMBO J* **13**, 675-682 (1994).
47. Johnson, D.B. *et al.* Melanoma-specific MHC-II expression represents a tumour-autonomous phenotype and predicts response to anti-PD-1/PD-L1 therapy. *Nat Commun* **7**, 10582 (2016).
48. Rodig, S.J. *et al.* MHC proteins confer differential sensitivity to CTLA-4 and PD-1 blockade in untreated metastatic melanoma. *Sci Transl Med* **10** (2018).
49. Gellrich, F.F., Schmitz, M., Beissert, S. & Meier, F. Anti-PD-1 and Novel Combinations in the Treatment of Melanoma-An Update. *J Clin Med* **9** (2020).
50. Zuazo, M. *et al.* Functional systemic CD4 immunity is required for clinical responses to PD-L1/PD-1 blockade therapy. *EMBO Mol Med* **11**, e10293 (2019).
51. Pirozyan, M.R. *et al.* Pretreatment Innate Cell Populations and CD4 T Cells in Blood Are Associated With Response to Immune Checkpoint Blockade in Melanoma Patients. *Front Immunol* **11**, 372 (2020).
52. Oh, D.Y. *et al.* Intratumoral CD4(+) T Cells Mediate Anti-tumor Cytotoxicity in Human Bladder Cancer. *Cell* **181**, 1612-1625 e1613 (2020).
53. Tay, R.E., Richardson, E.K. & Toh, H.C. Revisiting the role of CD4(+) T cells in cancer immunotherapy-new insights into old paradigms. *Cancer Gene Ther* (2020).
54. Kagamu, H. *et al.* CD4(+) T-cell Immunity in the Peripheral Blood Correlates with Response to Anti-PD-1 Therapy. *Cancer Immunol Res* **8**, 334-344 (2020).

55. Gentles, A.J. *et al.* The prognostic landscape of genes and infiltrating immune cells across human cancers. *Nat Med* **21**, 938-945 (2015).
56. Alam, M.S. Proximity Ligation Assay (PLA). *Curr Protoc Immunol* **123**, e58 (2018).
57. Norton, P. *et al.* Development and application of a novel recombinant Aleuria aurantia lectin with enhanced core fucose binding for identification of glycoprotein biomarkers of hepatocellular carcinoma. *Proteomics* **16**, 3126-3136 (2016).
58. Etzioni, A. & Tonetti, M. Fucose supplementation in leukocyte adhesion deficiency type II. *Blood* **95**, 3641-3643 (2000).
59. Marquardt, T. *et al.* Correction of leukocyte adhesion deficiency type II with oral fucose. *Blood* **94**, 3976-3985 (1999).
60. Liang, W. *et al.* Core Fucosylation of the T Cell Receptor Is Required for T Cell Activation. *Front Immunol* **9**, 78 (2018).
61. Okada, M. *et al.* Blockage of Core Fucosylation Reduces Cell-Surface Expression of PD-1 and Promotes Anti-tumor Immune Responses of T Cells. *Cell Rep* **20**, 1017-1028 (2017).
62. Alatrash, G. *et al.* Fucosylation Enhances the Efficacy of Adoptively Transferred Antigen-Specific Cytotoxic T Lymphocytes. *Clin Cancer Res* **25**, 2610-2620 (2019).
63. Keren, L. *et al.* A Structured Tumor-Immune Microenvironment in Triple Negative Breast Cancer Revealed by Multiplexed Ion Beam Imaging. *Cell* **174**, 1373-1387 e1319 (2018).
64. Nestarenkaite, A. *et al.* Immuno-Interface Score to Predict Outcome in Colorectal Cancer Independent of Microsatellite Instability Status. *Cancers (Basel)* **12** (2020).
65. O'Malley, D.P. *et al.* Immunohistochemical detection of PD-L1 among diverse human neoplasms in a reference laboratory: observations based upon 62,896 cases. *Mod Pathol* **32**, 929-942 (2019).
66. Cox, J. & Mann, M. MaxQuant enables high peptide identification rates, individualized p.p.b.-range mass accuracies and proteome-wide protein quantification. *Nat Biotechnol* **26**, 1367-1372 (2008).
67. Grabinger, T. *et al.* Alleviation of Intestinal Inflammation by Oral Supplementation With 2-Fucosyllactose in Mice. *Front Microbiol* **10**, 1385 (2019).
68. Smith, P.L. *et al.* Conditional control of selectin ligand expression and global fucosylation events in mice with a targeted mutation at the FX locus. *J Cell Biol* **158**, 801-815 (2002).
69. Wang, H. *et al.* D-mannose ameliorates autoimmune phenotypes in mouse models of lupus. *BMC Immunol* **22**, 1 (2021).
70. Wang, Y. *et al.* Loss of alpha1,6-fucosyltransferase suppressed liver regeneration: implication of core fucose in the regulation of growth factor receptor-mediated cellular signaling. *Sci Rep* **5**, 8264 (2015).
71. Zhang, D. *et al.* D-mannose induces regulatory T cells and suppresses immunopathology. *Nat Med* **23**, 1036-1045 (2017).

Tables

Tables 1 to 3 are available in the Supplementary Files section.

Figures

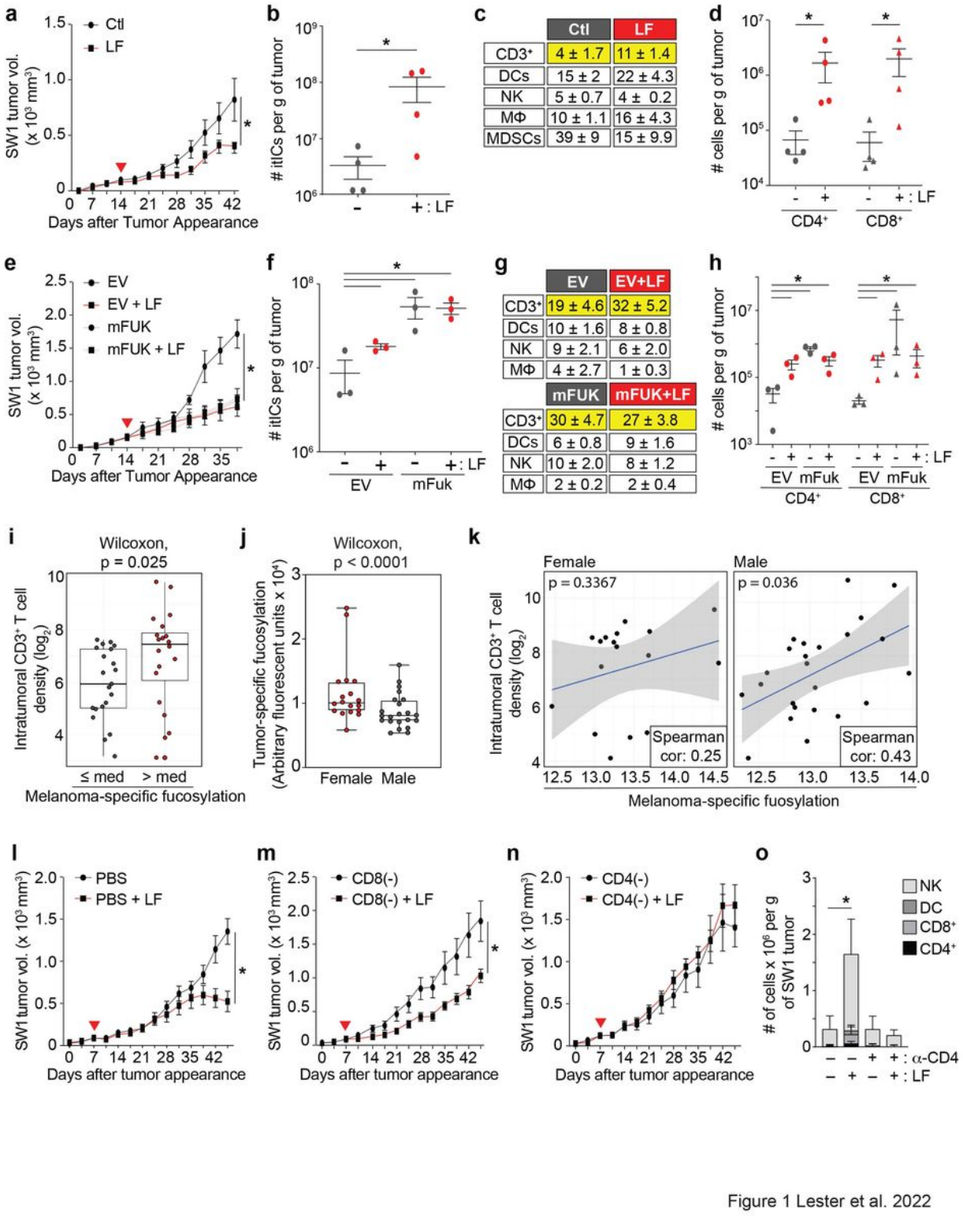

Figure 1 Lester et al. 2022

Figure 1

Increasing melanoma fucosylation reduces tumor growth and increases itIC abundance, particularly CD4⁺ and CD8⁺ T cells

Volumetric growth curves, total itIC counts, % itIC subpopulations ($CD3^+$ T cells, dendritic cells (DCs), natural killer cells (NKs), macrophages (MΦ), and MDSC-like (MDSC) cells), and intratumoral $CD3^+/CD4^+$ ($CD4^+$) and $CD3^+/CD8^+$ ($CD8^+$) T cell counts of SW1 tumors (**a, b, c, & d, respectively**) or of empty vector (EV)- or mouse fucokinase (mFUK)- expressing SW1 tumors (**e, f, g, & h, respectively**) in C3H/HeN mice. ▼ *= initiated L-fucose supplementation. The growth curves are means ± SEM from ≥7 mice per group. * = p<0.05.* **(i)** Association of melanoma-specific fucosylation and $CD3^+$T cell density (*log2 scale*) in a 41-patient melanoma tissue microarray. **(j)** Boxplots showing lower melanoma-specific fucosylation in male than female patients. **(k)** Scatterplots showing higher correlation between melanoma-specific fucosylation and $CD3^+$T cell density (log2 scale) is higher in male (Spearman's rho=0.43; *p=0.036*) than female (Spearman's rho=0.25; *p=0.3367*) patients. Volumetric growth curves for SW1 tumors in **(l)** PBS (control)-injected, **(m)** $CD8^+$T cell-, or **(n)** $CD4^+$ T cell-immunodepleted C3H/HeN mice. **(o)** Comparison of intratumoral NK, DC, $CD8^+$ T, and $CD4^+$ T cell subpopulations (absolute cell numbers) from tumors in **(l)** and **(n)**.

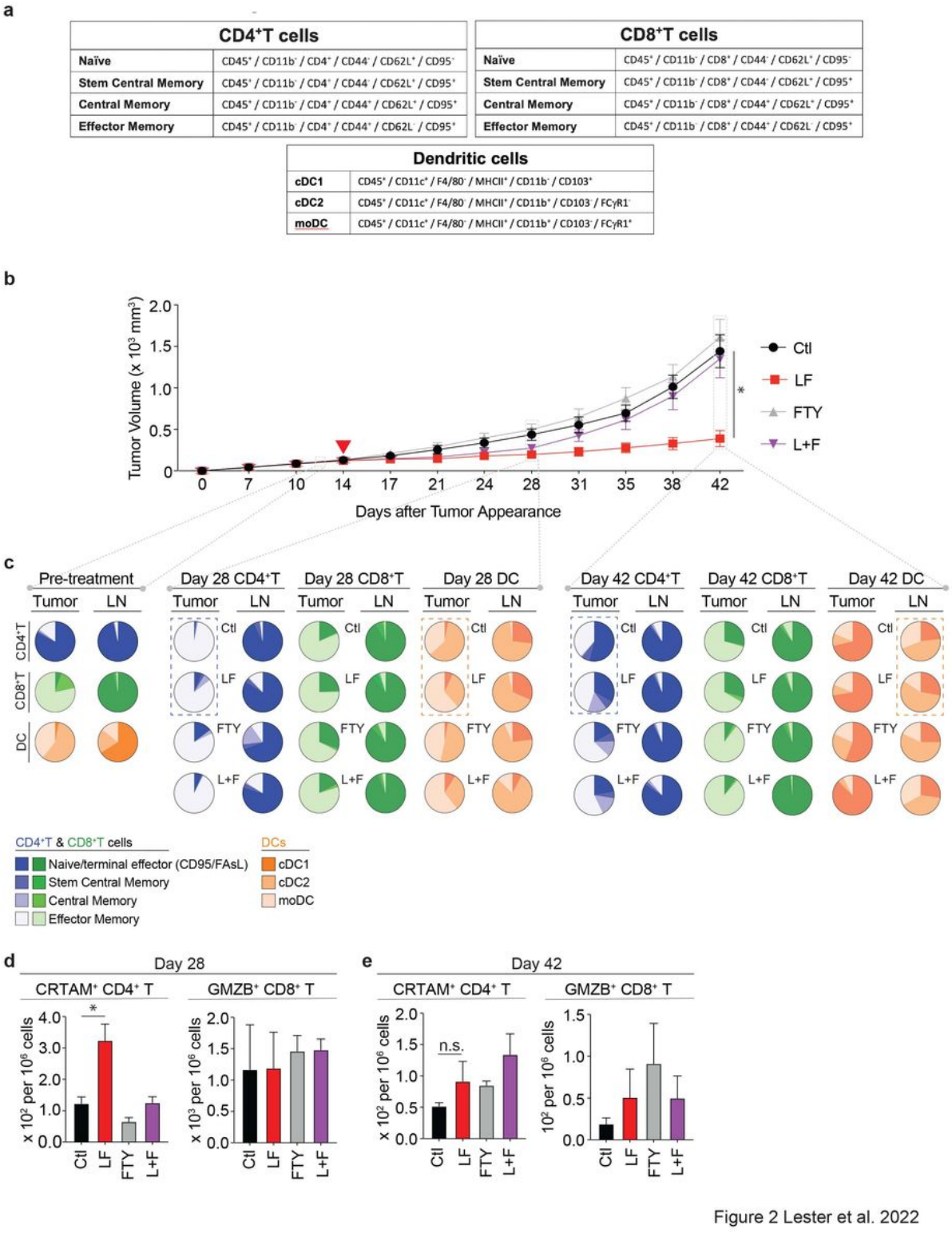

Figure 2 Lester et al. 2022

Figure 2

Lymph node egress is necessary for L-fucose-triggered tumor suppression; L-fucose increases intratumoral CD4+T stem and central memory cells.

(a) Immune subpopulations markers use to profile by flow cytometry. **(b)** Volumetric growth curves for SW1 tumors in C3H/HeN mice fed without (Ctl) or with L-fucose (LF) and treated with FTY720 (Ctl mice

administered FTY720: (FTY); LF-supplemented mice administered FTY720: (L+F)). FTY720 was administered at 20 µg per mouse every 2 days starting on Day 12, just prior to the initiation of LF **(c)** Pie charts showing ratios of intratumoral or lymph node-resident $CD4^+$ or $CD8^+$T cell subpopulations, as well as DC subtypes from mice at Day 14, 28, and 42 (each pie chart represents 4-5 mice). Assessment of cytotoxic $CD4^+$ T cell populations ($CRTAM^+$) and cytotoxic $CD8^+$ T cell populations ($GrzB^+$) from tumors at Day 28 **(d)** and Day 42 **(e)**. Corresponding raw flow cytometric data for these charts are shown in **Table 1**. *The tumor growth curves are means ± SEM from ≥7 mice per group. * = p<0.05.*

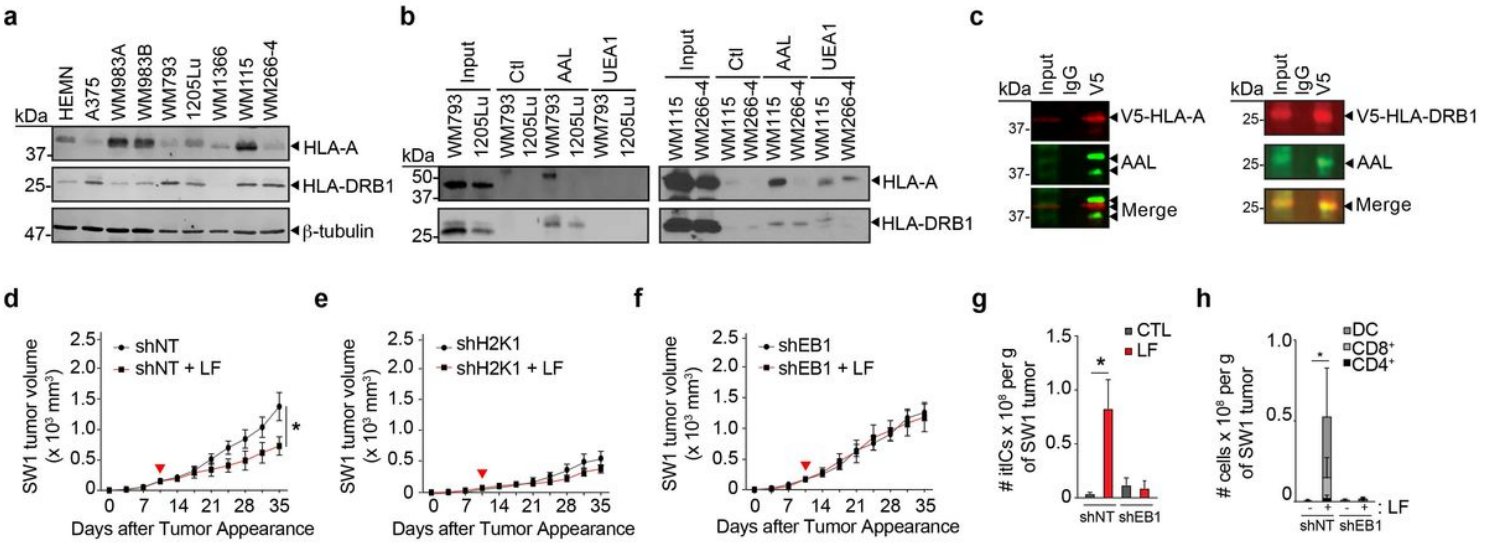

Figure 3 Lester et al. 2022

Figure 3

HLA-DRB1 is expressed, fucosylated, and required for L-fucose-triggered melanoma suppression and increased TIL abundance

(a) Immunoblot (IB) analysis of HLA-A and HLA-DRB1 levels in primary human melanocytes (HEMN) or indicated human melanoma cell lines. **(b)** Lectin pulldown (LPD) and IB analysis of patient-matched primary and metastatic cell line pairs WM793 and 1205Lu (*left*) and WM115 and WM266-4 (*right*) for HLA-A and HLA-DRB1. **(c)** V5-immunoprecipitation (IP) and IB analyses of WM793 cells expressing (*left)*

V5-tagged HLA-A or (*right)*V5-tagged HLA-DRB1. Volumetric growth curves for **(d)** non-targeting control shRNA (shNT)-, **(e)** H2K1-targeting shRNA (shH2K1)-, or **(f)**H2EB1-targeting shRNA (shEB1)-expressing SW1 tumors in C3H/HeN mice. Flow cytometric comparison of **(g)** total itIC counts or **(h)** indicated subpopulations from shNT- or shEB1-expressing tumors in **(d)**and **(f)**. *For* **(d-f)**, ▼ *= initiated L-fucose supplementation; growth curves are means ± SEM from ≥7 mice per group. * = p<0.05.*

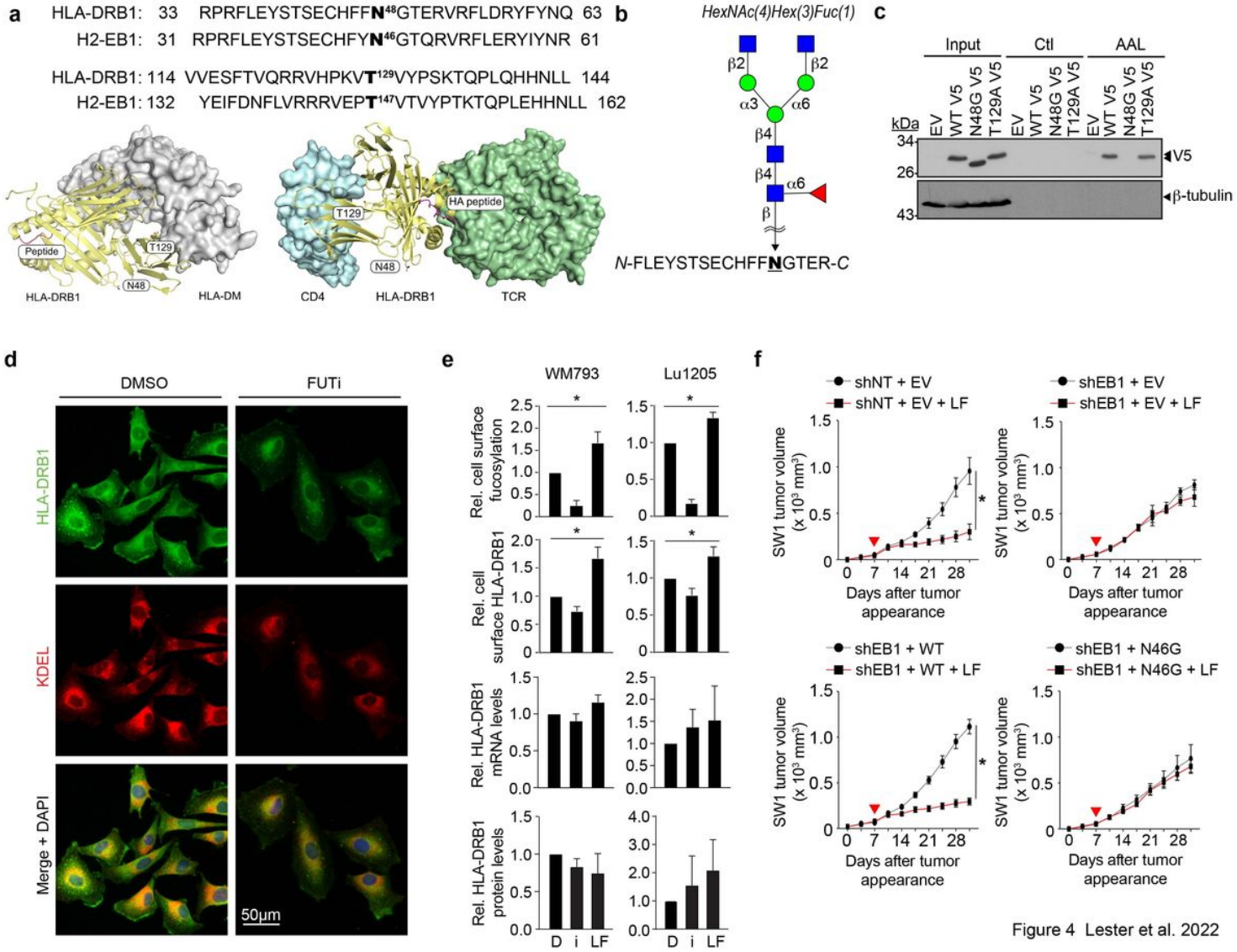

Figure 4 Lester et al. 2022

Figure 4

N-linked fucosylation of HLA-DRB1 at N48 regulates its cell surface localization and is required for tumor suppression and increased TIL abundance

(a) (*upper*) Amino acid sequence alignments showing conservation of predicted N- and O-linked fucosylation sites in human HLA-DRB1 (N48 and T129) and mouse H2EB1 (N46 and T147). Structural modeling of the HLA-DRB1:HLA-DM (*lower left*) and CD4:HLA-DRB1:TCR (*lower right*) complexes. Potential glycosylation sites, N48 and T129, of HLA-DR1 beta chain are shown as sticks. CD4 (cyan), HLA-DRB1 (yellow), antigen peptide (magenta), and TCR (green)(*lower right*). **(b)**HLA-DRB1 peptide

fragment identified by nano-LC/MS to be fucosylated on N48, with predicted HexNAc(4)Hex(3)Fuc(1) glycan structure shown above. **(c)** Lectin pull down (LPD) and IB analyses of EV and V5-tagged wild-type HLA-DRB1 (WT)-, HLA-DRB1 N48G (N48G)-, and HLA-DRB1 T129A (T129A)-expressing WM793 cells. **(d)** DMSO- or fucosyltransferase inhibitor (FUTi)-treated WM793 cells immunofluorescently stained for endogenous HLA-DRB1, KDEL (ER marker), and DAPI (*20x magnification*). **(e)** Flow cytometric analysis for relative cell surface fucosylation (*upper*) and cell surface HLA-DRB1 (*upper middle*), qRT-PCR analysis of relative HLA-DRB1 mRNA levels (*lower middle*), and IB analysis of HLA-DRB1 protein levels (*lower*) in WM793 and 1205Lu cells treated with DMSO (D), 250μM FUTi (i), or 250μM L-fuc (LF). **(f)** Volumetric growth curves for shNT (non-targeting shRNA) + EV (control SW1 tumors)(*upper left*) or shEB1 tumors reconstituted with EV (*upper right*), EB1 WT (*lower left*), or EB1 N46G (*lower right*) in C3H/HeN mice. *Control (grey) or L-fucose supplemented water (red, 100 mM; ▼ = initiated supplementation) was provided ad libitum. The tumor growth curves are means ± SEM from ≥7 mice per group. * = p<0.05.*

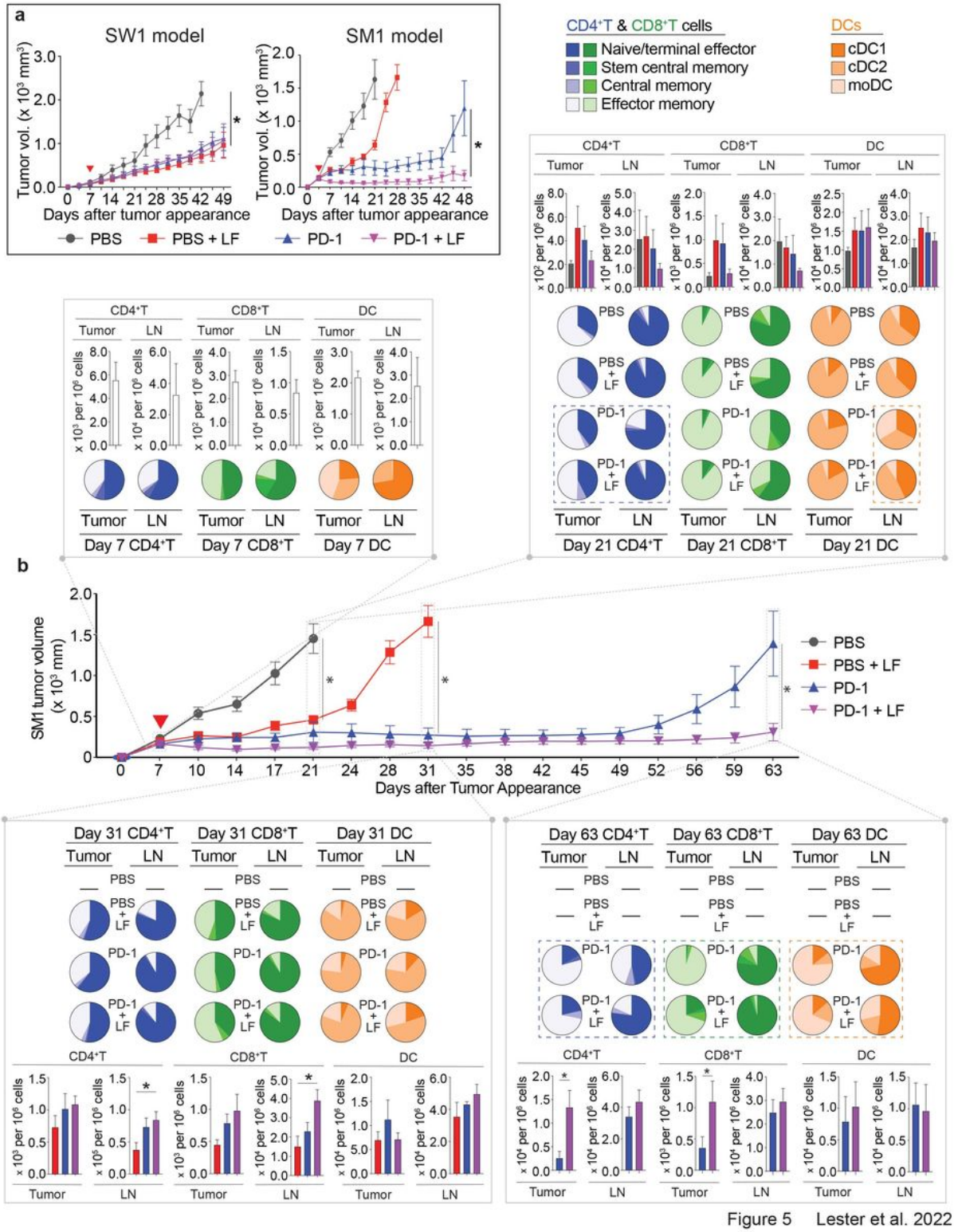

Figure 5 Lester et al. 2022

Figure 5

Administration of combination L-fucose and anti-PD-1 suppresses tumors and increases intratumoral CD4⁺ T central and effector memory cells

(a) Volumetric growth curves for SW1 tumors in C3H/HeN mice (*left*) and SM1 tumors in C57BL/6 mice (*right*) fed ± L-fucose (LF) and treated with PBS (control) or anti-PD-1. (concurrent initiation of LF ± anti-

PD1 (◤)). *The tumor growth curves are means ± SEM from ≥7 mice per group.* **(b)** Volumetric growth curves for SM1 tumors in C57BL/6 mice fed ± L-fucose (LF) and treated with PBS (control) or anti-PD-1 (PD-1). (concurrent initiation of LF ± PD1 (◤)). *The tumor growth curves are means ± SEM from ≥7 mice per group. * = p<0.05.* At Day 7 (prior to administration of LF or PD1), Day 21 (endpoint for tumors of control-treated mice), Day 31 (endpoint for tumors of LF-treated mice), Day 63 (endpoint for tumors of PD1-treated mice), the primary tumors (Tumor) and draining lymph nodes (LN) of 4-5 mice per treatment group were analyzed by flow cytometry for intratumor levels of $CD4^+$ and $CD8^+$ T subpopulations (naive/terminal, stem central/central/effector memory) and dendritic cell (DC) subpopulations (cDC1, cDC2, and monocyte-derived DC (moDC)) as in **Fig. 2**. Proportions of $CD4^+$, $CD8^+$, and DC subpopulations in each organ at each timepoints are represented by the color-coded pie charts (each pie chart represents 4-5 mice). Absolute numbers of the subpopulations per 10^6 cells of tumor/tissue homogenate at each timepoint are represented in the color-coded column charts. Corresponding raw flow cytometric data for these charts are shown in **Table 2**.

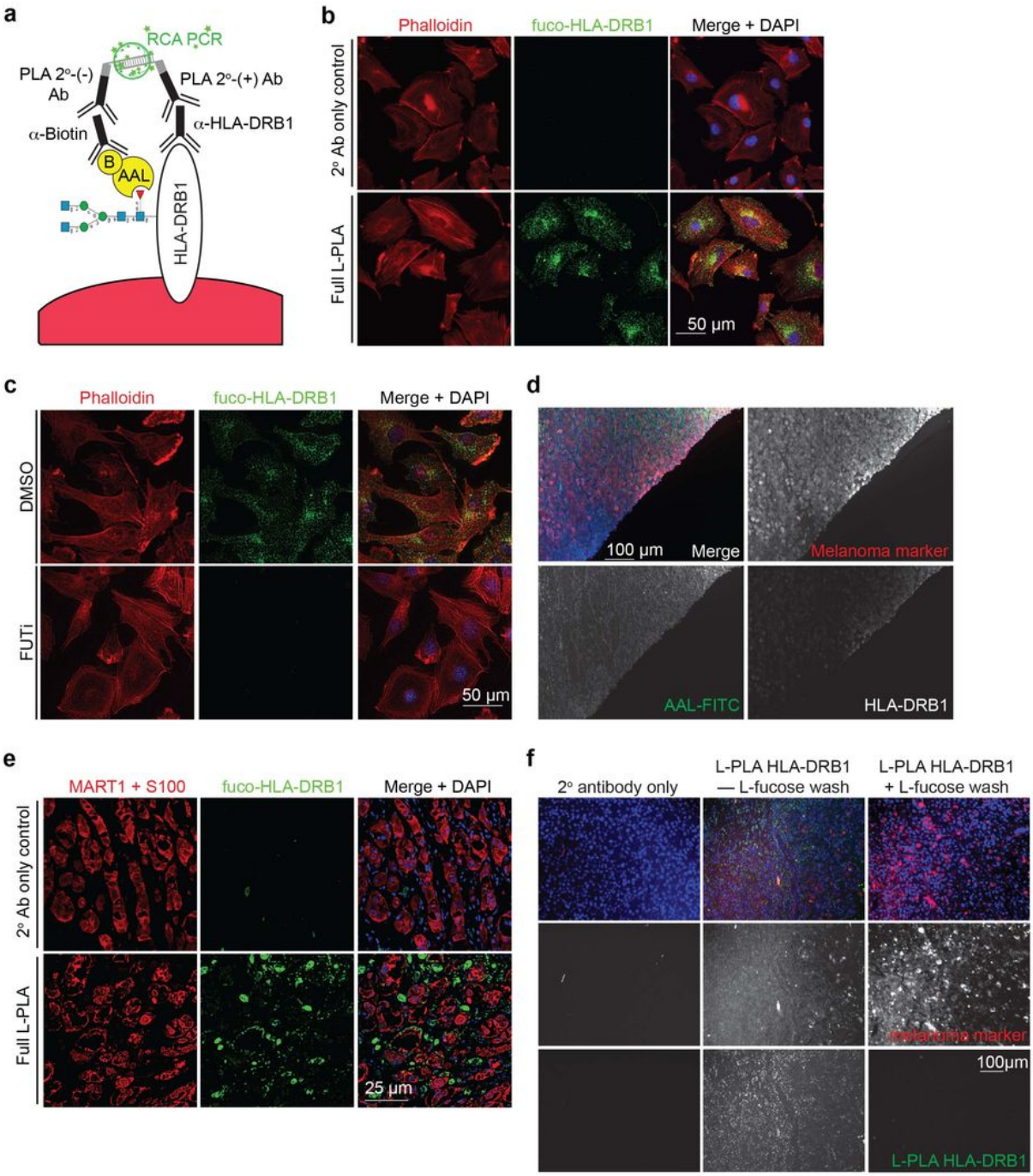

Figure 6 Lester et al. 2022

Figure 6

Immunofluorescent visualization of fucosylated HLA-DRB1: development of lectin-mediated proximity ligation technique

(a) Schematic of lectin-mediated proximity ligation analysis (L-PLA) using fucosylated HLA-DRB1 (fuco-HLA-DRB1) as an example. We stained for (i) HLA-DRB1 using a-HLA-DRB1 followed by (+) oligo-

conjugated PLA secondary and (ii) fucosylated glycan using biotinylated (“B”) AAL lectin followed by a-biotin followed by (-) oligo-conjugated PLA secondary. Ligated PLA oligos were subjected to rolling circle amplification PCR (RCA PCR), giving rise to fluorescent punctae. **(b)** Representative images of secondary antibody-only control (*upper*) or full L-PLA (*lower*) staining of endogenous, fucosylated HLA-DRB1 performed on coverslip-grown WM793 cells (with phalloidin and DAPIco-stains)
(c) To further demonstrate that fuco-HLA-DRB1 L-PLA staining is fucosylation species-specific, we performed L-PLA of endogenous, fuco-HLA-DRB1 on WM793 cells treated with DMSO or FUTi (phalloidin and DAPIco-stains). **(d)** To demonstrate specificity of individual L-PLA primary antibodies, FFPE melanoma tissue was stained for melanoma marker (MART1 + S100 cocktail), AAL-FITC, HLA-DRB1 (white), and DAPI. **(e)** Representative images of secondary antibody-only control (*upper*) or full L-PLA (*lower*) staining of endogenous, fucosylated HLA-DRB1 performed on human melanoma specimens (with MART1+S100 (melanoma markers) and DAPI co-stains). **(f)** FFPE melanoma tissues were subjected to L-PLA HLA-DRB1 staining ± 500mM L-fucose wash and subsequent staining with melanoma marker (MART1+S100 cocktail), and DAPI. Total loss of fuco-HLA-DRB1signal in the + L-fucose wash tissue confirms the fucose-specificity of L-PLA for fuco-HLA-DRB1. Single melanoma marker and fuco-HLA-DRB1 channels are shown in white for clear visualization.

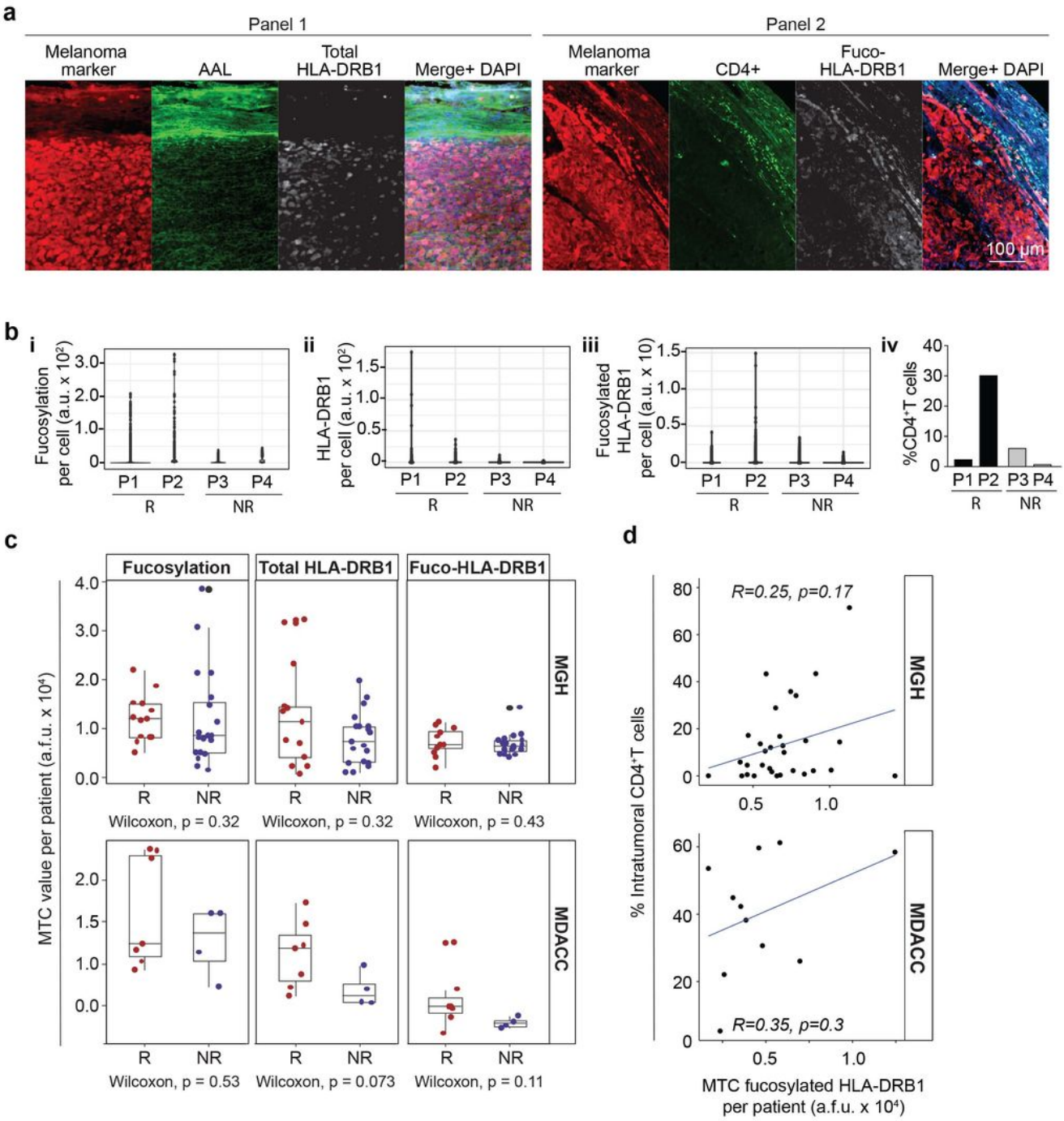

Figure 7 Lester et al. 2022

Figure 7

Clinical implications of melanoma fucosylation and fucosylated HLA-DRB1 for anti-PD1 in melanoma

(a) Representative images of anti-PD1-treated Moffitt patient tumors subjected to immunofluorescent staining for the 2 indicated panels of markers. **(b)** Dot plots showing single-cell distribution of **(i)** total fucosylation (AAL), **(ii)** total and **(iii)** fucosylated HLA-DRB1 staining intensities per melanoma cell, and

(iv) %CD4^{+}T cells (of total cells) within tumors of 2 responder (Pt. 1 & 2) and 2 non-responder (Pt. 3 & 4) Moffitt patients**. (c)** Box plots showing mean tumor cellular (MTC; means derived from single tumor cell intensities) fucosylation (*left*), total (*center*) and fucosylated (*right*; fuco-HLA-DRB1) HLA-DRB1 staining intensities of anti-PD1 responder (R; red dots) and non-responder (NR; blue dots) patients from (*upper*) Massachusetts General Hospital ((MGH); n=32) or (*lower*) MD Anderson Cancer Center ((MDACC); n=11). **(d)** % intratumoral CD4^{+}T cells (of total cells) plotted against corresponding average MTC fuco-HLA-DRB1 for each patient in the MGH (*upper*) and MDACC (*lower*) cohorts.

Supplementary Files

This is a list of supplementary files associated with this preprint. Click to download.

- SupplementaryInformation.pdf
- EXTENDEDDATA1.pdf
- EXTENDEDDATA2.pdf
- EXTENDEDDATA3.pdf
- EXTENDEDDATA4.pdf
- EXTENDEDDATA5.pdf
- EXTENDEDDATA6.pdf
- TABLE1.xlsx
- TABLE2.xlsx
- TABLE3.xlsx